Image Cover Sheet

CLASSIFICATION	SYSTEM NUMBER
UNCLASSIFIED	149012

TITLE

LONG RANGE AIRCRAFT DETECTION USING HIGH-FREQUENCY SURFACE-WAVE RADAR

System Number:

Patron Number:

Requester:

Notes:

DSIS Use only:

Deliver to: FF

National Defence / Défense nationale

LONG RANGE AIRCRAFT DETECTION USING HIGH-FREQUENCY SURFACE-WAVE RADAR

by

Hank Leong

DEFENCE RESEARCH ESTABLISHMENT OTTAWA
REPORT NO. 1245

Canada

December 1994
Ottawa

National Défense
Defence nationale

LONG RANGE AIRCRAFT DETECTION USING HIGH-FREQUENCY SURFACE-WAVE RADAR

by

Hank Leong
Surface Radar Section
Radar and Space Division

DEFENCE RESEARCH ESTABLISHMENT OTTAWA
REPORT NO. 1245

PCN
041LR

December 1994
Ottawa

Abstract

Experimental data from a High-Frequency Surface-Wave Radar (HFSWR) operating at 1.95 MHz at Cape Bonavista, Newfoundland are analyzed to assess the capability of the radar to detect aircraft over an ocean surface. The results of the analysis show that the HFSWR could easily detect and track a low-flying CP-140 Aurora aircraft at ranges between 11 and 56 km. The radar's coverage area coincides with a trans-Atlantic international flight route, and the radar was also able to detect and track some commercial aircraft in range as far as 280 km.

Résumé

Lors d'un essai d'un système radar décamétrique à ondes de surface opérant à la fréquence 1.95 MHz au Cap Bonavista à Terre-Neuve, on a fait une analyse en profondeur des données recueillies. Le but de cette analyse était d'évaluer la capacité de ce système à détecter et pister des avions volants au dessus de la mer. Lors de cette analyse on a démontré que l'on pouvait facilement détecter et pister un avion de type CP-140 Aurora volant à basse altitude à des distances variant entre 11 et 56 km. La région de veille pour ce radar inclut les routes des vols commerciaux transatlantiques. Donc, plusieurs avions commerciaux ont été détectés et pistés jusqu'à une distance de 280 km.

Executive Summary

The High-Frequency Surface-Wave Radar (HFSWR) trials were carried out at Cape Bonavista, Newfoundland in 1989 by NORDCO Limited [1]. The objective of the trials was to assess the capability of HFSWR to detect ship and low-flying aircraft targets at long ranges. A large amount of backscatter data were collected during the trials. These data are analyzed in this report to give some indication of the aircraft-detection capability of the HFSWR.

The backscatter data of the HFSWR include sea clutter and background noise. Dominant sea-clutter components are normally confined to a small region of low frequencies in the Doppler spectrum of the HFSWR. High-speed aircraft targets have Doppler shifts away from these sea-clutter components. Therefore, the conventional cell-averaging CFAR processing technique [2] can be adapted in the Doppler space to detect the aircraft targets. This technique, however, establishes the detection threshold on the basis of sample averaging. Large interference components in some Doppler cells of the HFSWR may increase the threshold in the others. This may result in undetected targets. In this report, we modify the conventional CFAR process. We use two threshold values: the first threshold is empirically set, and it is used to identify any Doppler cells that may contain large interference components; once these Doppler cells are excluded, the second threshold is then established by averaging the samples in the remaining cells. This second threshold is used for target detection.

A tracking algorithm is also implemented to automatically track the detected targets. This algorithm is relatively simple: it uses the detection algorithm above to initiate tracks and the velocity information of the detected targets to associate and maintain tracks. Because target azimuthal and elevation information is not available from the data, tracking is performed in range only.

Two aircraft were used as dedicated targets in the trials: a CP-140 Aurora and a CP-121 Tracker. The Aurora, the larger of the two, flew at an altitude of 1000 ft, and could be detected and tracked at ranges between 11 and 56 km. The path tracked from the HFSWR data is in good agreement with the data log from the trial. The Tracker, however, could not be conclusively detected because no target track could be established for the aircraft. Many targets of opportunity were detected and some were tracked in range as far as 280 km. These are likely the trans-Atlantic commercial aircraft which would arrive at or depart from Gander International Airport of Newfoundland, located only about 100 km northwest of the radar site. Detection of these targets clearly indicates the feasibility of using HFSWRs for long range aircraft detection.

Table of Contents

List of Figures

1. Introduction

Under contract to DND, NORDCO Limited carried out a series of trials [1] using a High-Frequency Surface-Wave Radar (HFSWR) at Cape Bonavista, Newfoundland. The objective of the trials was to assess the radar's capabilities for detecting ships and low-flying aircraft at long ranges. A large amount of radar backscatter were collected during the trials. To achieve the objective, we performed two different analyses for the backscatter data: the first analysis evaluates the radar's performance in ship detection, and the second evaluates the radar's capability for aircraft detection. The results of the first analysis have been presented in [3]. In this report, we present the results of the second analysis to give indications of the aircraft-detection capability of the HFSWR.

The backscatter data of the HFSWR include sea clutter and background noise. Sea clutter is caused by the interaction between HF radio waves and ocean waves. In the Doppler spectrum, sea clutter is characterized by a pair of first-order discrete components and a second-order continuum [4,5]. These sea-clutter components dominate a small frequency region around 0 Hz, and are superimposed on an essentially flat noise spectrum. In addition to sea clutter and white noise, the experimental HFSWR may also be subject to various forms of interference, and the interference signals may appear in the backscatter data.

Since aircraft normally have Doppler shifts in the frequency regions dominated by noise, detection of aircraft can be assumed to be noise-limited. In this report, we adapt the conventional cell-averaging Constant False Alarm Rate (CFAR) process [2] for the detection of aircraft targets in the noise environment. To guard against possible interference, we use two threshold values in the detection process. The first threshold is determined from the average of the samples in the frequency regions dominated by noise; it is used to screen out any large samples that might be caused by interference. After the large samples are excluded, the second threshold is established according to the conventional CFAR process; this second threshold is used for aircraft detection.

A tracking algorithm is also implemented to automatically track aircraft targets. This algorithm uses the detection algorithm above to initiate tracks and the velocity information of the detected targets to associate and maintain tracks. Because the azimuthal information is not available from the experimental radar, tracking is performed in range only.

Two dedicated aircraft were used in the trials: a CP-140 Aurora and a CP-121 Tracker. The Aurora, the larger of the two, flew at an altitude of 1000 ft, and could be detected easily at ranges between 11 and 56 km. The path tracked from the HFSWR data is in good agreement with the data log from the trials. The Tracker, however, could not be conclusively detected because no target track could be established for the aircraft. Many targets of opportunity were detected and some of them were tracked in range as far as 280 km. These targets are likely trans-Atlantic commercial aircraft which would arrive at or depart from Gander International Airport of Newfoundland, located only about 100 km northwest of the radar site.

2. The Experimental HFSWR

2.1 The Radar Facility

The HFSWR is a monostatic radar that comprises a LORAN A transmitter and a linear array receiver. The transmitter radiates omni-directionally at a frequency of 1.95 MHz with a peak power of 1 MW. It transmits a train of 50 μs pulses, shaped to a raised cosine, at a pulse repetition frequency (PRF) of 25 Hz. The receive array consists of eleven doublet antennas, each of which has an inter-element separation of one quarter wavelength (at 1.95 MHz). The antenna elements are evenly spaced along a line, with a separation of one half wavelength from one another. Figure 1 shows the theoretical and measured azimuth beam-patterns of the receive array. The uniformly weighted array has a theoretical beamwidth of 10°. Note that the measured beam-pattern is slightly asymmetrical along the boresight, which is 110° clockwise from the true North.

The signals received from the doublet antennas are summed coherently at radio frequency (RF), forming a beam along the boresight. The summed signal is then down-converted to an intermediate frequency (IF) of 25 kHz. At IF, the signal is sampled at a rate of 125 kHz (or 1 sample per 8 μs) with a 16-bit analog-to-digital converter (ADC). Note that the ADC has a dynamic range of 96 dB. The sampled data are recorded on 8 mm Exabyte cassette tapes, and then down-converted to the complex baseband with the preprocessing computer software developed at DREO [6]. Digital in-phase and quadrature mixing (I and Q channels) are used in the preprocessing to yield a complex discrete-time signal.

There are 507 samples in the discrete-time signal. These are called range samples because they are the radar echoes from various ranges. Since the sampling period of the ADC, Δt, is

8 μs, each range sample represents the backscatter of the radar from a range interval that is only 1.2 km wide (as defined by $c*\Delta t/2$, where c is the speed of light = $3x10^8$ m/s). The minimum range of the radar was set to 10 km approximately. Therefore, the maximum range of the radar would be 10 + 1.2*507, or 617 km.

A complex time series can be formed at a given range by collecting the corresponding range samples from consecutive radar pulses. The real and imaginary parts of the time series are from the I and Q channels. The effective sampling rate of these time series, f_s, is equal to the radar's PRF, i.e., 25 Hz.

Note that the ADC oversamples the radar signal at IF. The radar has a pulse width of 50 μs (3dB end-to-end), and a range resolution of 7.5 km (as defined by $c\tau/2$, where τ is the pulse width). This implies that the echo produced by a stationary point target would last for 50 μs, equivalent to 7.5 km in range. Since the radar return is sampled every 8 μs, the target echo will be in six or more (50/8) consecutive range samples (the exact number depends on the target signal strength). For HFSWRs, long coherent integration is often required to enhance the target signal-to-noise ratio and to determine the target radial velocity. The target echo will spread out even more in range if the target moves across range within the integration period. The target echoes from the consecutive range samples, however, will vary according to the shape of the transmitted pulse. Since the transmitted pulse is a raised cosine having a peak in the middle, the target echoes can be interpolated in range to give a more accurate estimate of the target range. In this report, we will consider the range at which the maximum target signal occurs as the target range for a given integration period.

2.2 The Data Acquisition

The trials were carried out during daytime on August 21-23, 1989. The sea condition can be described as calm on the first two and half days when the wind speed was between 4 and 6 m/s, and relatively rough on the second half of the third day when the wind speed was between 9 and 12 m/s. The times during which the data were collected are 10:18 - 18:53 on Aug. 21, 07:20 - 18:28 on Aug. 22 and 08:24 - 15:13 on Aug 23 (local time). A total of 60 data files were collected from the trials. For most of the data files, the radar's dwell time was 20 minutes. A log for some selected files is included in the Appendix. Note that the data files are numbered as DTxx with xx ranging from 01 to 60.

The two dedicated targets flew back and forth along the boresight of the HFSWR during the trials. The Tracker, the smaller of the two, was also used to verify and track other ship targets in the radar's coverage area. The Aurora normally has a speed of 300 knots (152 m/s) while the Tracker has a speed only between 120 and 150 knots (61 - 76 m/s). Upon approaching at these speeds, the Aurora has a Doppler shift of about 2 Hz in the Doppler spectrum and the Tracker has a Doppler shift between 0.8 and 1 Hz. The flight plans of the two aircraft are fairly extensive, and they can be found in Appendix J of [1].

2.3 Target Detection through Doppler Analysis

Target detection is achieved by first Doppler processing the finite-length time series, and then comparing the Doppler component with a threshold. Doppler processing is performed via the Fast Fourier Transform (FFT) algorithm. The length of the time series is determined by the integration period of the radar. The optimum integration period depends on the dynamics of the target of interest. If the target of interest has a constant radial velocity, then the optimum integration period should be equal to the duration over which the target travels across a range cell. However, if the target of interest has a rapidly-changing radial velocity, the optimum integration period needs to be reduced in order to determine the time-fluctuation of the radial velocity. For the processing of the current set of HFSWR data, we use an integration period of 40.96 seconds, which is optimum for the Aurora aircraft travelling at 300 knots along the boresight. If a target is found to have a rapidly-changing radial velocity, the integration period is shortened to 10.24 seconds. At 25 Hz PRF, the radar would have transmitted 1024 pulses (N=1024) in 40.96 seconds. Figure 2 shows the Doppler Spectra of four 1024-point time series from the HFSWR at different ranges. Note that a Blackman window [7] has been applied to the time series before the application of the FFT. The Blackman window attenuates the first sidelobes to about 58 dB below the main lobe in the Doppler spectrum.

A strong target signal can be observed at -1.978 Hz in Figure 2(a). This is the signal of an aircraft travelling away from the radar at a speed of 152 m/s, and it is likely that of the CP-140 Aurora. According to the pilot's log, the aircraft flew at about the same speed and at about the same range and the same time as indicated in Figure 2(a). Because the ADC oversamples the transmitted radar pulse, this target signal will appear across more than 6 consecutive range samples (see Section 2.1). To provide a more accurate estimate of the target range, it is necessary to interpolate the target signal across the range samples. Figure 3 show a plot of the target signal strength vs. range sample number. From this plot, a signal peak can be observed

at range sample #31. This signal peak indicates that the range of the target is 47.2 km (10 + 31*1.2), which should be accurate to within 1.2 km.

The dominant sea clutter can be observed in all the Doppler spectra in Figure 2. The two "sharp" lines on the left and right sides of the ground clutter at 0 Hz in Figure 2(a,c,d) are the first-order sea echo caused by a direct resonant scatter of the transmitted radar signal from ocean waves with a wavelength exactly equal to one half of the radar wavelength [4]. This resonant scatter is often referred to as Bragg scatter, in analogy to the X-ray diffraction mechanism in crystals. The resonant waves that produce the two sharp lines are surface waves travelling either toward or away from the radar on the ocean patch defined by a radar cell. The two sharp lines have unique Doppler shifts [4] at

$$f_B = \pm \sqrt{\frac{g}{\pi \lambda_r}} \qquad (1)$$

where g is the gravitational acceleration, or 9.81 m/s^2, and λ_r is the radar wavelength. For a radar operating at 1.95 MHz, $f_B = \pm 0.143$ Hz. These are called Bragg lines, representing the backscatter from the advancing and receding ocean waves.

The radar signal may also be scattered several times before returning to the radar receiver. The scattering points can be located on or off the ocean patch defined by a radar cell. The scattering mechanism at each point is similar to the Bragg scatter. The backscattered signal will become part of the sea clutter at a particular range if the time for the signal to return to the radar receiver is the same as the direct signal. The multiple scattering results in a sea-clutter continuum in the Doppler spectrum. Of particular significance is the second-order sea clutter resulted from a double scatter by the ocean waves. Srivastava and Walsh [5,8] have developed a comprehensive theoretical model for the second-order sea clutter. This model classifies the second-order sea-clutter into three parts according to the locations of the two scattering points:

(i) Both scattering points are on the ocean patch defined by a radar cell;
(ii) One scattering point is near the transmitter, and the other is on the ocean patch defined by the radar cell;
(iii) Both scattering points are off the ocean patch.

The sea clutter from the three double scatters are simply referred to as the first, second and third parts of the second-order sea clutter respectively. This model has been incorporated into

HFRADAR [9], a DREO simulation program for HFSWRs.

The theoretical Doppler spectra of the different sea clutter components are shown in Figure 4 for a 1.95 MHz HFSWR operating under a fully developed sea condition (wind speed: 30 knots; wind direction: 45° from the boresight). Note that the term "fully-developed sea" refers to a steady-state sea condition where the wind supplies just enough energy to the water to compensate for the energy lost in wave breaking and other dissipations [10]. As shown in Figure 4, the spectra of the various sea-clutter components are largely confined to the Doppler interval between -1 and 1 Hz for the 1.95 MHz HFSWR. The only possible exception is the second part of the second-order sea clutter. Under the fully developed sea condition, this part of the sea clutter rolls off slowly as the Doppler frequency increases (in magnitude).

The measured Doppler spectra in Figure 2, however, do not seem to show the characteristics of the second-order sea clutter. This is because the sea was not fully developed at the time the data were collected. The resonant waves have a fairly long wavelength (λ_r = 154 m for the radar, and λ_w = 77 m for the water). Strong wind is required to fully develop the ocean waves having such a long wavelength. At the time DT15 was acquired, the wind speed was only about 5 m/s or 10 knots, and the resonant waves were probably not even excited in the waters around the transmitter. Further discussion on the fully developed sea condition is given in Section 5.3.

3. Data Quality and Data Conditioning

A number of anomalies were found in the HFSWR data. The nature of the anomalies have been discussed in [6]. In this section, we will briefly describe the anomalies and discuss qualitatively the effects of these anomalies on aircraft detection. Some of the effects can be mitigated by data conditioning. In this section, we will also point out the procedure taken to mitigate these effects.

3.1 Noise Spikes

Large, impulse-like, noise spikes sometimes appear in the time series. These noise spikes raise the noise level in the Doppler spectrum, and reduce the signal-to-noise ratio of a target. Therefore, the noise spikes must be removed before the spectral analysis can be carried out.

An algorithm based on the amplitude distribution of a sinewave-like time series was developed in [3] to detect and remove the noise spikes. In the algorithm, an isolated noise spike is replaced with the average of the preceding and trailing samples, while contiguous noise spikes are replaced with the RMS value of the samples in the time series (excluding those considered as noise spikes). This spike-attenuation algorithm has proven to be fairly effective, and it is applied to the time series.

3.2 60 Hz harmonic Interference

As shown in Figure 5, spectral peaks can be observed at ±5 and ±10 Hz in the Doppler spectrum that spans from -12.5 to 12.5 Hz. These spectral peaks are likely caused by the interference of 60 Hz harmonics that are present in the AC power supply of the HFSWR. The 60 Hz harmonics modulate the dominant sea-clutter components and produce spectral replicas at those frequencies. The spectral replicas are aliased [11] into the Doppler spectrum because they are under-sampled. Aliasing causes a spectral component located at frequency f before sampling to appear at f_a = MOD (f, f_s) after sampling. The spectral replicas which would be located at ±60 Hz, ±120 Hz, ±180 Hz, etc. are therefore centred at one of the four frequencies: ±5 and ±10 Hz.

Most aircraft have speeds less than 300 m/s, which corresponds to a Doppler shift between -4 and 4 Hz in the Doppler spectrum. Therefore, the presence of the spectral replicas at the higher frequencies should not pose a serious problem in the detection of these targets. However, the spectral replicas may change the noise and sea-clutter statistics of the radar, and in some cases, they may even raise the noise floor in the Doppler spectrum. Therefore, some degradation in the aircraft-detection performance is expected.

An algorithm based on the optimization of the spectral power of the interference was developed in [12] to suppress the 60 Hz harmonics. This algorithm has the promise of suppressing the harmonics without adversely altering the noise and sea-clutter statistics in the HFSWR data. However, the algorithm relies on adequate modelling of the interference harmonics. In the HFSWR data, the fundamental frequency of the interference harmonics often fluctuates with time. A large number of parameters are required to model the interference. Consequently, the algorithm may become numerically complex. This complexity makes it impractical to apply the algorithm to the large amount of data.

3.3 Ionospheric Reflection

It is well known that HF radio waves can be reflected back to the earth by the ionosphere because of the ionization of gas particles by solar radiation and other high-energy particle emission from the sun [10]. The ionosphere is generally divided into D, E and F layers, corresponding to altitude bands of 50-90, 90-130, and 130-350 km respectively. The doublet antennas used in the HFSWR at Cape Bonavista have a wide elevation coverage. Therefore, the reflections of the transmitted signal from the ionosphere may be included in the return of the radar. The ionospheric reflections are range-dependent. Hence, it is necessary to plot the Doppler components as functions of range to observe the interference. The Doppler components of interest here are the power of the sea-clutter continuum, $P_{s,h}$, and the noise power-density, P_n. Figure 6 shows the two Doppler components as functions of range using the data from the twenty-first integration period of file DT15. At a given range, $P_{s,h}$ is obtained from an incoherent sum of the Doppler samples from -1 to 1 Hz, excluding those around the Bragg lines and 0 Hz, while P_n is estimated from an incoherent sum of the Doppler samples in the noise-dominated regions, i.e., between -4 and -1 Hz and between 1 and 4 Hz. Note that because of the harmonic interference at ±5 Hz and ±10 Hz, the Doppler samples beyond ±5 Hz are not used in the estimation of P_n.

Normally, a monotonic decrease is expected in the profile of $P_{s,h}$. However, in Figure 6(a), two strong peaks are now observed at around 102 km and 227 km respectively. The range of the first peak is in the altitude band of the E-layer, while the range of the second peak is slightly more than twice the range of the first. Consequently, one can infer that the two strong peaks are likely caused by a direct reflection and a second-round reflection of the transmitted radar signal from the E-layer in the ionosphere. The second-round reflection occurs when the radar signal is reflected first downward from the E-layer, then upward from the sea surface, and finally downward from the E-layer to the radar receiver. Figure 7 illustrates the possible paths for the direct (first-round) and second-round reflections. A Doppler spectrum subject to the interference of the ionospheric reflection is shown in Figure 2(b).

The noise power-density profile in Figure 6(b) does not show any strong peaks around 102 and 227 km. This indicates that, in this particular data file, the ionospheric reflections are confined to the Doppler interval between -1 and 1 Hz. Therefore, if one is interested in detecting targets with absolute Doppler frequencies greater than 1 Hz, or with radial speeds greater than 77 m/s, the ionospheric reflections should not have much effect on the detection in this data file.

However, the ionospheric reflections are not always confined to (-1, 1 Hz), and they could adversely affect the detection of aircraft with low radial velocities. This will be discussed further in Section 5.5.

3.4 Receiver Blanking

Digital bandpass and lowpass filters are used in the preprocessing of the HFSWR data. These are delay-line Finite-Impulse-Response (FIR) filters. At the beginning of each radar pulse, the taps of the filters are filled with zeroes (hence referred to as receiver blanking), and these filters will not be in steady state for the first few samples. Therefore, the amplitudes of the very first few samples will increase with range, as indicated in Figure 6.

If a target is located at the very close-in ranges, the target return may exhibit similar increases. In this case, the interpolation method described in Section 2.3 will be ineffective for target range estimation.

3.5 Slow Roll-off of Sea-Clutter Continuum at Close-in Ranges

The site of the HFSWR was chosen to facilitate the observation of the second part of the second-order sea clutter, as described in Section 2.3. The radar transmitter is located on the tip of the Cape Bonavista peninsula. Therefore, the transmitted signal may be scattered forward by the ocean waves around the transmitter, and then backward to the receiver by the ocean waves in a given radar cell. Experimental evidence has been provided for the presence of the second part of the second-order sea clutter by Srivastava and Ponsford [13] from the data collected from the HFSWR under very rough sea conditions caused by Hurricane Dean on Aug. 8, 1989.

The sea condition was relatively calm during the trials on Aug. 21-23. However, the sea-clutter continuum sometimes still shows the slow roll-off characteristic from the dominant Bragg lines and from the spectral replicas at ±5 Hz in the measured Doppler spectrum at close-in ranges. This is evident in Figure 5 where the portions of the Doppler spectrum from which the noise power-density was estimated become slightly concave up. Because of this slow roll-off, P_n would over-estimate the noise power-density at close-in ranges. As shown in Figure 6(b), P_n is higher at close-in ranges; it increases and then decreases with range before it becomes constant at about 60 km. The slow roll-off of the sea clutter could degrade the radar performance at the close-in ranges, particularly in the detection of the CP-121 Tracker.

3.6 Interference of Unknown Origin

Strong, target-like, signals sometimes appear in the noise-dominated regions in the Doppler spectrum. Likely caused by external interference or other system operations, these signals could last for a few minutes and appear across all the range cells. The effects of these signals on aircraft detection are:

(i) They will likely cause false alarms in the Doppler cells in which they appear.

(ii) If these signals are included in the averaging process commonly used to determine the detection threshold, they may raise the detection threshold in adjacent Doppler cells, and hence result in undetected targets.

4. Detection and Tracking of Aircraft Targets

4.1 Detection Algorithm

An automatic detection algorithm must be developed to efficiently search for targets in the massive amount of data. This requires establishing a threshold level in the Doppler space to achieve a desired probability of detection without exceeding a certain probability of false alarm. This threshold level depends on the statistics of the samples in the Doppler regions in which target signals are likely to appear. Since aircraft targets normally have Doppler shifts in the frequency regions dominated by noise, we will only consider the statistics of noise spectral components in this report.

Because of the presence of the 60 Hz harmonics, we shall confine the search for aircraft targets nominally in the Doppler regions of (-4, -1 Hz) and (1, 4 Hz). This effectively excludes the Doppler regions dominated by sea clutter and the 60 Hz harmonic interference from consideration. The Doppler frequencies of 1 and 4 Hz correspond to radial speeds of 77 and 308 m/s respectively. The majority of aircraft have radial speeds no more than 308 m/s. However, slow aircraft (e.g., the CP-121 Tracker), or aircraft travelling at an angle with the boresight, may have radial speeds less than 77 m/s. If we want to detect aircraft targets with low radial speeds, we need to lower the boundary frequencies, say, from ±1 Hz to ±0.75 Hz respectively. Note the boundary frequencies of ±1 Hz have been chosen such that the sea clutter is mostly confined to

the interval of (-1, 1 Hz). In the Doppler regions of (-1, -0.75 Hz) and (0.75, 1 Hz), noise is still in contention with sea clutter, and often noise will dominate, particularly at long ranges.

Let M denote the total number of the samples in the two noise-dominated Doppler regions, and x_i, i=1,2,3, ..., M, be the squared magnitudes of these samples. Since we only deal with the squared magnitudes in the detection algorithm, we will simply call x_i as the sample in the following. For an integration period of 40.96 seconds at a PRF of 25 Hz, M is equal to $1024*\Delta f_d/25$, where Δf_d is the total length of the noise-dominated Doppler intervals. If the boundary frequencies are ±1 and ±4 Hz, then M equals to 246.

In the absence of target signals or interference signals, the x_i can be assumed to have independent exponential distributions:

$$f(x_i) = \frac{1}{\mu_x} \exp\left(-\frac{x_i}{\mu_x}\right) \qquad 0 \le x_i < \infty \tag{2}$$

where μ_x is the mean value of x_i. For a given threshold value X_T, the probability of false alarm P_{fa} is:

$$P_{fa} = \int_{X_T}^{\infty} f(x)\, dx = \exp\left(-\frac{X_T}{\mu_x}\right) \tag{3}$$

This threshold value can be expressed in terms of P_{fa}:

$$X_T = -\mu_x \ln(P_{fa}) \tag{4}$$

To determine the threshold, we must find the mean value μ_x. If the distributions of all x_i are identical for i=1,2,3, ..., M, then the conventional cell-averaging CFAR processing technique [2] can be used, i.e., for each Doppler cell, the mean value μ_x can be approximated by the average of the samples in its adjacent Doppler cells. For example, for Doppler cell n, this average is given by

$$\bar{\mu}_n = \frac{1}{M-3}\left(\sum_{i=1}^{n-2} x_i + \sum_{i=n+2}^{M} x_i\right) \tag{5}$$

or

$$\bar{\mu}_n = \frac{1}{M-3}\left(\sum_{i-1}^{M} x_i - (x_{n-1}+x_n+x_{n+1})\right) \tag{6}$$

Note that the samples in cells n-1 and n+1 are also excluded from the average to guard against the signal spread from the n-th cell. The two cells are hence called guard cells.

The distributions of x_i, however, are not always identical for i=1,2,3, ..., M because interference and sometimes target signals may be present in the Doppler spectrum. The samples due to the interference or target signals are much larger than the other samples in the two Doppler intervals. Inclusion of these samples in Equation (5) will overestimate the mean values for the other Doppler cells in the two Doppler regions. This overestimation will increase the threshold values for the Doppler cells, and therefore may result in undetected targets.

To reduce the number of undetected targets, we modify the cell-averaging CFAR process. We will use two threshold values: the first threshold is used to identify the larger samples that may be caused by interference in the data, and the second threshold, obtained after the larger samples are excluded, is used for target detection.

The first threshold, V_T, is empirically set. It is determined from Equation (4) with the mean value μ_x being replaced by the average $\bar{x}$ of all the M samples in the two Doppler intervals:

$$V_T = -2\,\bar{x}\,\ln(P_{fa}) \tag{7}$$

Note that a factor of 2 has been added to the equation to ensure that only a few samples are identified as "large samples". This factor is arbitrary, but it should be greater than unity.

Let p be the number of the samples exceeding the first threshold (p << M), and x_{Lj}, j=1,2, ..., p, be those samples. For the remaining samples, we adapt the conventional CFAR processing technique, i.e., for the n-th remaining cell, the mean value μ_x in Equation (4) can be approximated by

$$\bar{\mu}_n = \frac{1}{M-p-3}\left(\sum_{i=1}^{M} x_i - \sum_{j=1}^{p} x_{Lj} - (x_{n-1}+x_n+x_{n+1})\right) \tag{8}$$

This equation will be applied to all the remaining Doppler cells except those at the end points of the two Doppler intervals. For the end points, there are two alternatives to obtain the estimate:

either we include one extra sample from outside the two Doppler intervals (so that we can use the equation above), or we simply ignore the guard cell outside the Doppler intervals, and use

$$\bar{\mu}_n = \frac{1}{M-p-2}\left(\sum_{i=1}^{M} x_i - \sum_{j=1}^{p} x_{Lj} - (x_n+x_{n+1})\right) \tag{9}$$

for the left end points of the intervals, and

$$\bar{\mu}_n = \frac{1}{M-p-2}\left(\sum_{i=1}^{M} x_i - \sum_{j=1}^{p} x_{Lj} - (x_{n-1}+x_n)\right) \tag{10}$$

for the right end points of the intervals.

For the n-th cell, the second threshold value, V_{Tn}, is given by:

$$V_{Tn} = -\bar{\mu}_n \ln(P_{fa}) \tag{11}$$

This threshold value will be established for each remaining Doppler cell in the two frequency regions.

A block diagram for the detection algorithm is shown in Figure 8. Note that the algorithm calls Subroutine THRESH to determine the second threshold values V_{Tn} for all Doppler cells in the two frequency regions. This actually is not necessary for the samples that exceed the first threshold, as they will be considered as possible target samples. However, for the ease of programming, one can still apply it to the large samples. This application should not change the outcome for the samples because V_{Tn} is smaller than V_T.

The detection algorithm described here is essentially the same as that in [2] except here we have added the first threshold to give some tolerance for interference and the possibility of multiple targets in the Doppler spectrum. The performance of this algorithm, therefore, should be the same as that in [2], provided that the algorithm is applied in the noise-dominated regions. However, when the sea clutter is in contention with the noise, some degradation in false alarm rate and detection performance is expected. In particular, when the sea-clutter continuum rolls off slowly into the frequency regions normally dominated by noise, the samples near the end points of the two Doppler regions may cause false alarms.

4.2 Tracking Algorithm

The HFSWR collects data continuously. Therefore it is possible to track targets in range over time. Since the radial velocity of a target can be deduced from the Doppler frequency in one integration period, one can predict where the target will be in the next integration period by assuming the target maintains constant velocity. In the neighbourhood of the predicted location, one can then use the detection algorithm to confirm the presence of the target. By repeating this process over consecutive integration periods, a target track can be established.

This simple form of tracking provides the backbone for the algorithm described in this section. Designed mainly for single targets, the algorithm can also be used for multiple targets if Doppler separations among the targets are sufficiently large. Figure 9 shows a block diagram for the algorithm. The key blocks in the algorithm are: track initiation, range refinement, target-range estimation, track association, track termination and track validation. The functionality of each block is described as follows:

1) Track Initiation -- Subroutine DETECT

In a given integration period, DETECT uses the algorithm in Section 4.1 to determine if any of the Doppler cells in the frequency intervals of (-4, -1 Hz) and (1, 4 Hz) contains a possible target signal. A target signal may spread over several contiguous Doppler cells, and multiple targets may also exist in the Doppler spectrum. DETECT determines the number of possible targets by counting the number of local maxima in the Doppler cells that are already declared as containing possible target signals. In the case of multiple targets, DETECT also determines the Doppler separations between the target signals ($2\Delta f$), which will be used in subroutine DETWTR for track association.

2) Range Refinement -- Subroutine MAXRD

DETECT only gives coarse estimates of target ranges because the target return may appear across several neighbouring range samples. MAXRD is used to improve the accuracy of the target range estimates. Once a target is detected, MAXRD searches for the maximum target signal in a localized neighbourhood of the estimated range and Doppler frequency. This localized neighbourhood extends 6 km (5 range samples) on either side of the estimated range and Δf on either side of the target Doppler. The value

of Δf is user-specified, but it will be changed in the case of multiple targets to half the Doppler separation between adjacent target signals.

3) Target-range Estimation

The radial velocity of a target can be estimated from the Doppler shift of the target in a given integration period. By assuming the target maintains constant radial velocity, one can estimate the distance the target will travel in the next integration period. By adding this distance to the range of the target in the given integration period, one can then predict what the range of the target will be in the next integration period. This prediction localizes the target range, and hence minimizes the probability of forming the track with other detected targets in the next integration period.

4) Track Association -- Subroutine DETWTR

DETWTR stands for DETect-While-TRack. At the predicted range, DETWTR uses MAXRD to search for the maximum target signal in the next integration period, and then calls the detection algorithm to verify the presence of the target. If the target is confirmed to be present near the predicted range, then DETWTR associates this new detection with the track.

In the case of multiple targets, DETWTR takes a simple approach to distinguish the various tracks: it limits the maximum Doppler change of a target over an integration period to a value no more than half of the Doppler separation(s) between the target and its adjacent target(s) in the Doppler spectrum. This is a restrictive approach. It works only if the Doppler separations between any of the targets are sufficiently large.

The case of multiple targets rarely occurs in the current HFSWR data. It is often interference that causes the apparent appearance of multiple targets. Fortunately, in these rare cases, there are sufficient Doppler separations for the tracking algorithm. Examples of multiple target-like signals in the same Doppler spectrum will be shown in Section 5.5.

5) Track Termination

Theoretically, a track can be terminated when the target is not detected in an integration

period. However, because the radar antenna has a fairly strong sidelobes, the target may disappear in the null between the main lobe and the sidelobe, and then appear again in the sidelobe. We have initially assumed that a track is terminated when the target is not seen by the radar, but we found that some targets appear again after one or two integration periods. Subsequently, we changed the termination condition: we kept tracking until the end of a data file to include the possibility of the sidelobe appearance.

6) Track Validation

Since the HFSWR was subject to various interference, false target tracks may have been established. Track validation can eliminate some of these tracks. There are two validation methods. One is to check the length of a track, and the other is to check the range and radial velocity along a track.

The radar dwells for a long time and covers a large area. Hence, a target with a Doppler shift in the two specified intervals must move across several range cells over consecutive integration periods. If a target track is too short, then it becomes questionable. In this report, we assume that a target track is not established unless the target is observed over at least two integration periods.

The relationship between the range and radial velocity along a track must follow the fundamental physics: the range increment should be equal to the travelled distance estimated from the radial velocity and the integration time, at least approximately. For example, if a target has a radial velocity of 100 m/s, it would have travelled 4.1 km in 40.96 seconds. If the range of the target indicates that it has travelled 20 km instead, then the track becomes questionable and should be discarded.

The criteria for the second validation depend on the dynamics of the targets. It is difficult to establish a firm set of criteria for all aircraft targets. Consequently, the validation is not performed in the algorithm, and all the tracks are left for the user to interpret.

An established track contains the following information on a target: the target signal strength, range and radial velocity in different integration periods. Note that the tracking is performed in range only.

5. Results and Discussions

All the data collected during the three-day period have been analyzed with the detection algorithm and the tracking algorithm. Unless otherwise specified, the integration period for Doppler processing is 40.96 seconds. For detection, the probability of false alarm is set to 10^{-5}. For tracking, it is assumed that a target track is established only if it is observed in at least two consecutive integration periods.

Many aircraft are observed in the HFSWR data. The majority of these are targets of opportunity. The data files in which aircraft are detected include: DT05, DT15, DT16, DT17, DT18, DT19, DT37, DT39, DT51, DT52 and DT57. All these data files were acquired in the afternoon during the three days of trials. The data collected in the early afternoon on the first day (DT06 - DT14) were corrupted due to a malfunctioning of the Timing Control Unit (TCU) of the radar; no targets can be detected from these data.

The CP-140 Aurora, one of the two dedicated aircraft targets, was detected and tracked from DT15 during Run #3 both when it went away from the radar and when it came back towards the radar. Runs #1 and #2 were carried out in the early afternoon of the first day when the TCU was malfunctioning, and the aircraft could not be detected.

As reported in [1], the CP-121 Tracker could not be conclusively detected from the current set of data because there were no established tracks for the target. The Tracker is smaller and slower than the Aurora. This implies that the signal of the Tracker is weaker, and appears closer to the dominant sea clutter. The Tracker had a speed between 120 and 150 knots, corresponding to a Doppler shift between 0.8 Hz and 1.0 Hz only. Sometimes, the Tracker zigzagged at 45° from the boresight of the radar, and its Doppler shift became even smaller, i.e., between 0.56 Hz and 0.71 Hz. At these Doppler frequencies, the sea-clutter continuum is still fairly dominating, especially at close-in ranges. Consequently, the Tracker could not be detected.

In the following, we will concentrate on two of the data files, DT15 and DT39, to give a detailed analysis of the target detection using the HFSWR. The two data files were acquired at about the same time, but on two different days: DT15 on Aug. 21 between 14:24 and 14:44 NDT; DT39 on Aug. 22 between 14:12 and 14:32 NDT. The dwell time for each data file was 20 minutes (1200 seconds). The dedicated aircraft targets were used in both data files: in DT15,

the Aurora started Run #3 with 1023 seconds remaining, and the Tracker started Run #4 with 750 seconds remaining; in DT39, the Tracker started Run #7 with 1032 seconds remaining.

Figure 10 shows the recorded flight path of the Aurora in Run #3: the aircraft flew outbound from 6 nm (11.1 km) to 30 nm (55.6 km) at an altitude of 1000 ft, turned around and then came back along the boresight of the radar. The Tracker had a similar flight pattern during Run #4: it flew outbound from 6 nm to 60 nm at an altitude of about 200 ft along the boresight of the radar. The Tracker flew at an altitude of 1000 ft during Run #7. The outbound portion of Run #7 is essentially the same as that of Run #4, but along the inbound portion, the Tracker zigzagged at 45° from the radar boresight. Both aircraft were asked to bank as sharp as possible at the far ranges to give maximum airframe exposure to the radar beam.

5.1 Target Tracks In DT15

Detection of aircraft targets in DT15 was carried out in the Doppler intervals between -3.75 and -0.75 Hz, and between 0.75 and 3.75 Hz. Figure 11 shows the target tracks along the boresight of the radar. Note that the time in Figure 11 is referenced to the beginning of the data file. At close-in ranges, the Aurora was tracked between 10 and 70 km, both inbound and outbound. At far ranges, two inbound aircraft were tracked between 150 and 280 km. The numbers marked along the Aurora track correspond to those marked along the recorded track in Figure 10. As indicated, the estimated Aurora track agrees very well with the recorded. The two inbound aircraft are likely trans-Atlantic commercial flights. They can be detected at far ranges because of their large radar cross-sections (RCS) and their high altitudes. Note that the Tracker was not detected in this data file.

Figure 11 also shows that, within an integration period, a target can be detected across several neighbouring range samples. The small "crosses" in Figure 11 indicate targets detected from the Doppler spectra by the detection algorithm. In a given integration period, they can be observed across several contiguous range samples. At close-in ranges, in particular, the target signals are so strong that they may appear across more than 10 range samples. By interpolating the target signals in range, however, the tracking algorithm was able to locate the targets with a range accuracy of 1.2 km.

Many detected targets (the small "crosses") in Figure 11 cannot be linked together to form tracks. These are most likely false alarms caused by sea clutter or some other external

interference. The tracking algorithm eliminates these false alarms on the basis that they do not form continuous tracks. Examples of the false alarms will be given in Section 5.5.

The Aurora aircraft changed direction three times; it turned around at about 100, 500 and 900 seconds respectively. During the time it turned around, the radial velocity and hence the Doppler frequency of the aircraft changed considerably in 40.96 seconds. To keep pace with the changing velocity of the target, we shortened the integration period to 10.24 seconds and re-processed the data. Figure 12 shows the new track for the Aurora aircraft along with the corresponding radial velocity. As shown in Figure 12, more frequent estimates are now obtained for the range and radial velocity of the Aurora aircraft. The aircraft is now clearly seen turning around at about 100, 500 and 900 seconds.

However, it should be pointed out that portions of the Aurora track in Figure 12 have been manually connected because the target could not be automatically detected for several short intervals along the track:

(i) The aircraft could not be detected once between 500 and 520 seconds and twice between 780 and 930 seconds (NB: the integration periods was 10.24 seconds). During these time intervals, the Aurora turned around and its Doppler dropped below 0.75 Hz. Because the target signal now appeared in the sea-clutter continuum, the detection algorithm could not be used.

(ii) The target was also undetected for several integration periods between 530 and 600 seconds because the HFSWR time series was corrupted with noise spikes. The spike-attenuation program [3] could not detect the noise spikes because they were in the same order of magnitude as the signal samples in the time series.

(iii) The target was detected during the first time it turned around. For most of the time interval between 50 and 180 seconds, the absolute Doppler frequency of the target was well above 0.75 Hz. However, because of receiver blanking, the target signal power increases with range for the first few range samples, and the interpolation method cannot be used to pinpoint the target location. In Figure 12, we have estimated the target ranges by assuming the target maintained a constant radial velocity. This estimated portion of the track is shown in Figure 12 with a dashed line.

The Aurora track in Figure 11 is shown in detail in Table I. The estimated ranges in Figure 11 are not absolutely calibrated yet, and they may be shifted by a constant. In Table I, we have used the recorded flight information of Run #3 to obtain a calibration constant. The aircraft started Run #3 at 16:56:55 GMT as shown at Location 1 in Figure 10. It flew away from the radar at a constant speed of 152 m/s from 6 nm (11.1 km) to 30 nm (55.6 km). This corresponds very well to the portion of the established track between 143 and 471 seconds in Table I. In fact, the distance the aircraft has travelled (44.5 km) is almost identical to the difference between the ranges at 143 and 471 seconds (44.4 km). Therefore, it can be concluded that the target detected at 143 seconds was at Location 1 on the map, and that the true target range at that time was 11.1 km, which is 9.7 km closer than the estimated range in Figure 10. This difference is used to calibrate the other estimated ranges from the HFSWR.

The recorded speed of the Aurora aircraft is 300 knots (154 m/s). The estimated radial velocity on the outbound leg is 152 m/s, which agrees well with the recorded. However, on the inbound leg approximately between 550 and 850 seconds, the estimated radial velocity is smaller than 300 knots and decreases with time. Since the Aurora came back along the radar boresight, this indicates that the aircraft slowed down on its way back.

The ranges and radial velocities of the other two targets are shown in Figure 13. The two targets were tracked almost continuously except (i) Target #1 was missed for two integration periods at about 400 seconds, and (ii) Target #2 was missed for one integration period at about 880 seconds. Note that the integration period is 40.96 seconds in Figure 13. The Doppler frequencies of the two targets along the tracks were well above 0.75 Hz. Hence, the missed detections are not due to low Doppler frequencies. This will be explained in Section 5.4.

Table I Aurora Track (run #3)

Data File: DT15 Acquisition Time (GMT): 16:54-17:24, August 21, 1989

IP[1]	Time (s)	Range Sample#	Range (km)	Velocity (Hz)	Velocity (m/s)	Signal Power[2] (dBu)	GMT	Cal. Range[3] (km)	Map Location
1	20	13	25.6	1.660	128	19.0	16:54:52	15.9	
2	61	10	22.0	1.855	143	17.4			
3	102	6	17.2	1.685	129	2.0[a]			
4	143	9	20.8	-1.880	-145	26.0	16:56:55	11.1 (6 nm)	1
5	184	11	23.2	-1.978	-152	26.4			
6	225	15	28.0	-1.978	-152	28.6			
7	266	20	34.0	-1.953	-150	26.3			
8	307	26	41.2	-1.978	-152	24.5			
9	348	31	47.2	-1.978	-152	21.2	17:00:05	37.5	2
10	389	36	53.2	-1.953	-150	18.3			
11	430	41	59.2	-1.978	-152	16.4			
12	471	46	65.2	-1.978	-152	20.9[b]	17:02:23	55.5 (30nm)	
13	512	47	66.4	-0.854	-66	-9.5[a]			
14	553	46	65.2	1.953	150	3.4[a]			
15	594	43	61.6	1.563	120	-8.5[a]			
16	635	38	55.6	1.514	116	9.3	17:05:06	45.9	3
17	676	33	49.6	1.489	115	18.6			
18	717	30	46.0	1.270	98	21.1			
19	758	27	42.4	1.196	92	11.8			
20	799	24	38.8	0.903	70	12.7			
21	840	21	35.2	0.681	45	7.0[c]			
22	881[d]								
23	922	16	29.2	1.343	103	12.0	17:09:53	19.5	
24	963[d]						17:10:34		4
25	1004	15	28.0	-1.831	-141	41.5	17:11:24	18.3	

Comments:

1 IP = Integration Period of 40.96 seconds or 1024 radar pulses.

2 The target signal power was estimated from an incoherent sum of the three samples at the target Doppler.

3 Ranges were calibrated according to the recorded flight information from run #3.

a When the target turns around, the target signal spreads out in the Doppler spectrum, and the three-point sum of the Doppler samples does not represent the true value of the signal power.

b At IP=12, the target slows down. The target signal power here was calculated from an incoherent sum of 16 Doppler samples.

c The target Doppler is below 0.75 Hz at 840 seconds, and the detection was made manually from the Doppler spectrum.

d The target was not detected at 881 and 963 seconds because of sea-clutter dominance.

5.2 Target Tracks In DT39

Detection of aircraft targets in DT39 was also carried out in the Doppler intervals between -3.75 and -0.75 Hz, and between 0.75 and 3.75 Hz. Figure 14 shows the established target tracks. Eleven targets of opportunity were detected in this file. The two targets at close-in ranges (#1 and #2) are particularly interesting in that they approached the radar together at about the same speed, and changed their heading at about the same range. The other targets tracked in this data file are likely commercial aircraft. All except two of them (#9 and #10) flew toward the radar. Note that there were many false alarms made by the detection algorithm in DT39, but they were rejected by the tracking program.

The two longest tracks at the far ranges (#4 and #5) are very similar to those from DT15 (#1 and #2). DT15 and DT39 were acquired at about the same time on two consecutive days, at 14:24 and 14:14 hours respectively. Therefore, the two tracks are likely those of two regular trans-Atlantic commercial flights. By comparing the tracks from the two different days, we found that both flights almost maintained their courses except that they came in a little earlier in DT39 than in DT15. Target #4 from DT39 arrived about 10 minutes earlier than Target #2 from DT15 while Target #5 from DT39 arrived about 3 minutes earlier than Target #1 from DT15. As a result, the two tracks in Figure 14 for DT39 appear to have switched positions from those in Figure 11 for DT15.

The radial velocities of Target #1 and #2 are shown in Figure 15. Upon turning, the radial velocities changed from about 180 to -180 m/s in 250 seconds. Because of the rapid velocity changes, a smaller integration period must be used at the time the aircraft turned around. A 256-point FFT has been used, instead of the normal 1024-point FFT.

The radial velocities of the other targets in DT39 are shown in Figure 16. Since all the estimated radial velocities exceed the maximum expected speed of the Tracker, we conclude that the Tracker is not among the detected targets in DT39.

5.3 Signal Strength and RCS Estimation for the CP-140 Aurora

Since the HFSWR at Cape Bonavista was not calibrated, the RCS of the aircraft cannot be estimated directly from the target signal. However, the RCS can be estimated indirectly by comparing the target signal with the Bragg lines. For a target near the sea surface with a free space RCS of σ_T, the power available at the radar receiver is given by [14,15]:

$$P_{rT} = \frac{P_t G_t G_r \lambda^2 |W|^4}{(4\pi)^3 R^4} \sigma_T \qquad (12)$$

where P_t = transmitted power

G_t, G_r = transmitter and receiver antenna gains, including the propagation effect of the sea surface

λ = free space radar wavelength = c/f_r, where f_r is the radar operating frequency

W = ground-wave attenuation factor, including sea-surface roughness

R = Target range

Similarly, from the sea surface of the ocean patch in a given range cell with a free space RCS of σ_S, the received power is given by:

$$P_{rS} = \frac{P_t G_t G_r \lambda^2 |W|^4}{(4\pi)^3 R^4} \sigma_S \qquad (13)$$

For the radar at Cape Bonavista,

$$\sigma_S = \sigma_0 \, R \, (\Delta\theta) \, (\Delta R) \qquad (14)$$

where σ_0 = scattering coefficient of the sea, or RCS of the sea per unit area

$\Delta\theta$ = half-power beamwidth of receiver antenna = 10°

ΔR = range resolution of the radar = 7.5 km.

A division of Equation (12) by (13) yields

$$\frac{P_{rT}}{P_{rS}} = \frac{\sigma_T}{\sigma_S} \qquad (15)$$

Hence, the RCS of the target σ_T can be estimated from Equation (15) if the scattering coefficient of the sea is known for the sea condition in which the HFSWR data were measured. Note that in deriving Equation (15), we have ignored the space wave components from an elevated target. The Aurora aircraft flew away from 11.1 to 55.5 km at an altitude of 1000 ft (approximately 300 m), and was within the radar horizon[1]. Therefore, space wave components, namely the direct wave and the reflected wave from the sea surface, were also present in the target signal. The space wave components, however, are much weaker than the surface wave. A study carried out in [1] indicates that at 1.95 MHz under a fully developed sea condition, the propagation loss to a target elevated at 300 m at a range of 30 km differs by no more than 1 dB from the propagation loss to a target at the sea surface at the same range. Hence, the space wave components are negligible as compared to the surface wave for the Aurora aircraft.

The sea scattering coefficient has been theoretically calculated [14] and experimentally measured [17] to be -29 dB for a fully developed sea condition. Strong wind must be sustained for tens of hours and over hundreds of kilometres to fully develop the resonant waves. According to the Phillips model for the ocean wave spectra [14], the smallest wave number of the sea that is excited at a wind speed u is:

$$k_{cut\text{-}off} = \frac{g}{u^2} \qquad where \quad k = \frac{2\pi}{\lambda_w} \tag{16}$$

For the resonant ocean wave to be excited, the minimum wind speed required is given by:

$$u_{\min} = \sqrt{\frac{g\lambda_r}{4\pi}} \tag{17}$$

where $\lambda_w = \lambda_r/2$ has been used for the resonant wave. For the 1.95 MHz radar, the minimum wind speed required is 11 m/s.

At the time the Aurora aircraft was detected, the wind speed was only about 5 m/s, and the sea was nowhere near being fully developed. Therefore, the power of the sea clutter obtained

---

[1]As given by $d = \sqrt{2kRh_r} + \sqrt{2kRh_t}$ [16], where kR is the effective radius of the earth, h_r (about 50 ft) and h_t are the heights of the radar and target respectively. At an altitude of 1000 ft, the radar horizon is 87.8 km.

from DT15 cannot be used in Equation (15) in conjunction with the known scattering coefficient of -29 dB to estimate the RCS of the Aurora. The best estimate that can be obtained during the three days of trials is from the data collected from the second half of the third day when the wind speed reached up to 12 m/s. Figure 17 shows the power of the Bragg lines from DT51 and DT52 collected respectively at 11:36 and 11:58 NDT on the third day. Bragg lines are known to have a large temporal variation [10]. To reduce this temporal variation, we have averaged the total power of the two Bragg lines in each Doppler spectrum over all the integration periods in DT51 and DT52.

The signal power of the outbound Aurora aircraft in DT15 is also shown in Figure 17. This signal power was estimated from an incoherent sum of the three samples at the target Doppler frequency in every integration period except the very last one. In the last integration period, the Aurora changed direction, and its Doppler spread out considerably. In Figure 17, we have estimated the target signal power in the last integration period from an incoherent sum of 16 samples. From the signal power of the target and the power of the Bragg lines, we can now use Equation (15) to estimate the RCS of the Aurora aircraft at the target ranges. These estimates are also shown in Figure 17 along with the RCS of the sea under a fully developed sea condition. Note that all the ranges used in Figure 17 have been calibrated by using the calibration constant from Section 5.1. Figure 17 shows:

(i) at a range between 18 and 35 km, the RCS of the aircraft was constant at about 8.6 dBm^2.

(ii) beyond 35 km, it increased gradually until it reached 18.5 dBm^2 at 56 km.

(iii) The RCS was smaller before 18 km; it is only between 3.5 and 5 dBm^2, which is about half of the value between 18 and 35 km.

The results of (i) and (ii) agree well with the manoeuvre taken by the aircraft along the track. The aircraft flew away initially with its tail directly facing the radar, and then, it banked toward the radar to increase the area of reflection. As shown in Figure 17, this is exactly what was observed: the RCS of the aircraft was constant first, and then increased gradually at the far ranges of the track. However, the result of (iii) cannot be explained with the target manoeuvre. The smaller RCS at the very close-in ranges is probably caused by the transient effect of receiver blanking at those ranges.

The agreement between the results of (i) and (ii) and the target manoeuvre gives confidence to the RCS estimates. However, as applied here, there are still problems with the estimation method:

(i) Even in DT51 and DT52, the sea may not be fully developed yet because the stronger wind has not blown for long enough. This would result in higher estimates for the aircraft RCS.

(ii) The scattering coefficient σ_0 (-29 dB) is valid for a homogeneous or semi-isotropic sea condition, and it does not include the effect of ocean swell. Given the geography of the radar site, it is likely that there is a significant swell component, particularly at the close-in ranges. This might also have an effect on the RCS estimates at the close-in ranges.

5.4 Correlation between Target Signal Strength and Antenna Beam-Pattern

In Section 5.1, we pointed out that the two commercial aircraft in DT15 sometimes went undetected for one or two integration periods. Figure 18 shows the signal strengths of the two targets along their tracks. These signal strengths indicate that these targets might not have been detected because of weak receiver antenna gains at their azimuths. As shown in Figure 18, the signal strengths do not increase monotonically with time although the ranges of the two aircraft decrease monotonically. This implies that the targets might have travelled at an angle off the radar boresight. As the targets traversed the receiver antenna beam, the variations of the antenna gain might have lead to the fluctuations of the target signals.

The range-dependence of the signal strengths in Figure 18 can be removed by calibrating the signals to the same (arbitrary) range according to Equation (12). The radar equation can be re-written as

$$G_r(\theta) = \left(\frac{(4\pi)^3}{P_t G_t \lambda^2 |W|^4 \sigma} \right) R^4 P_r \qquad (18)$$

Since the ground-wave attenuation factor W for a 1.95 MHz HFSWR is almost constant within the ranges of the targets [1], the term in the brackets of the equation above would be a constant if the RCSs of the targets are assumed to be constant along their tracks. If the received power P_r is adjusted with the range factor R^4, then we can obtain the receiver antenna gain at a function

of the target azimuth θ (in terms of the constant). Figure 19 shows the signal strengths of the two targets after being adjusted by the range factor. Since the two aircraft travelled across the antenna beam, the range-corrected signals map out part of the antenna beam-pattern.

Some measurements of the antenna beam-pattern have been given in Figure 1. This beam-pattern can be correlated with the range-corrected signal to yield the azimuthal information of the target. One way to carry out the correlation is to minimize the difference between the calibrated signal and the measured beam-pattern with respect to the azimuth of the target. However, because the target azimuth changes with time, it is normally difficult and impractical to solve this minimization problem. Besides, the solution to this problem may not be unique because there is only a limited number of data points available for the range-corrected signal and the measured beam-pattern.

Instead of solving the minimization problem, we will try to take advantage of the characteristics of the measured antenna beam-pattern. Since the aircraft target was likely in a cruising mode at long ranges, we will assume (i) the target had a constant heading and (ii) any signal change due to target elevation is negligible. To track the target in the two-dimensional space of range and azimuth, we need to determine an initial target azimuth and the heading of the target. Since the antenna beam-pattern has a peak value at a known azimuth, there must be a peak value in the range-corrected signal if the target has gone across the boresight. This peak value, evident in Figure 19, can then be used to determine the initial target azimuth. Once the initial azimuth is determined, the other azimuths of the target along the track can be estimated sequentially by comparing the range-corrected signal with the antenna gain. At the beginning of the estimation, the range-corrected signal strength may equal to the antenna gain at either side of the main lobe of the antenna beam-pattern. However, since the measured antenna beam-pattern is asymmetrical, one can quickly find that the range-corrected signal would not match one side of the antenna beam-pattern, and subsequently, obtain an estimate for the azimuth of the target with a constant heading. For example, starting from the peak of the range-corrected signal of Target #2 in DT15 at about 470 seconds, the range-corrected signal strength only follows the measured antenna beam-pattern at azimuths less than 110°.

The estimated azimuth and the range together constitute a two-dimensional track. Figure 20 shows the track for the target estimated after about 470 seconds. In Figure 20, the range and the estimated azimuth in polar coordinates have been converted to the distance along the boresight (R_x) and the distance vertical to the boresight (R_y) in rectangular coordinates. Note that

the HFSWR experimental site is at the origin of the coordinates. As shown in Figure 20, the estimated track follows closely along a straight line at an angle off the boresight. This confirms that the target indeed had a constant heading.

The range-corrected signal strength is shown in Figure 21 as a function of the estimated azimuth in the polar coordinates. This signal track clearly shows that the target has traversed the main lobe, the first side-lobe and part of the second side-lobe of the antenna beam-pattern. Comparison of Figures 1, 11 and 21 confirms the failure to detect the target at about 880 seconds was indeed caused by the weak antenna gain at the target azimuth. Similar situations occurred with Target #1 in DT15 at about 400 seconds and several targets in DT39.

5.5 Effects of Residual Anomalies on Aircraft Detection

In Section 3, we have pointed out that the effects of the various anomalies in the data on aircraft detection can be mitigated by data conditioning (e.g. noise spike removal). However, data conditioning before Doppler analysis works to a certain extent. In this subsection, we will point out some of the anomalies that still remain in the data, and we will also discuss how the detection and tracking algorithms will perform if these anomalies are present.

(a) Noise Spikes

The noise spikes are the most detrimental to target detection. They may raise the noise floor in the Doppler spectrum and result in undetected targets. The spike-attenuation program [3] is effective in most cases. However, when the noise spikes are as strong as some other signal samples in the time series, it is difficult to detect them automatically. Typical cases of undetected noise spikes are: (1) positive noise spikes, as strong as the peak-to-peak value of the sinusoidal time series, appear in the valley of the sinusoid, and (2) negative noise spikes, also as strong in magnitude as the peak-to-peak value of the sinusoidal time series, appear at the peak of the sinusoid.

The undetected noise spikes may lead to undetected targets. For example, in the 14th integration period in DT15, the Aurora aircraft could not be detected unless the noise spikes are manually removed. The Doppler spectrum of this time series is shown in Figure 22 before and after the manual removal of the noise spikes. As shown in Figure 22, the noise level becomes

considerably lower after the noise spikes are removed, and the target can now be detected by the algorithm of Section 4.1.

The effect of noise spikes is particularly pronounced if the target has a rapidly fluctuating radial velocity. A shorter segment is required to determine the speed fluctuation of the target. This implies a much higher noise level due to the noise spikes.

(b) 60 Hz Harmonic Interference

Because we have excluded from consideration the Doppler intervals of (-12.5, -4 Hz) and (4, 12.5 Hz), the 60 Hz harmonic interference does not pose a serious problem in the detection of aircraft targets. However, it affects the radar performance. The interference sometimes becomes so severe that it raises the noise floor in the Doppler spectrum and results in undetected targets. The interference also changes the noise statistical distribution in the Doppler spectrum, and eliminates almost any possibility of obtaining the noise statistics from the data.

In the case of a relatively fast target with a strong echo in the radar receiver, the replica of the target signal by the ±120 Hz harmonics may result in false alarms. In Figure 23(a), for example, the strong target return at about 2.45 Hz is replicated at about -2.55 Hz in the Doppler spectrum. Although the replicated target signal is weaker than the true target signal, it is still about 15 dB higher than the noise level, and will likely cause a false alarm in the detection algorithm. Incidently, Figure 2(a) illustrates a similar case.

(c) Ionospheric Reflection

The ionospheric reflections are not always confined to a smaller Doppler region around 0 Hz. Sometimes they may spread into the higher Doppler regions in the Doppler spectrum. Figure 23(b) shows one such Doppler spectrum from the 21st integration period of DT20, acquired at about 18:00 NDT, only 2.5 hours later than DT15. While the ionospheric reflections are confined in DT15 between -1 and 1 Hz, the first-round ionospheric reflection in DT20 has now extended almost up to ±2 Hz. The power of the the sea-clutter continuum ($P_{s,h}$) and the noise power-density (P_n) from the same integration period of DT20 are plotted in Figure 24 as functions of range. Unlike the noise profile for DT15 in Figure 6(b), the noise profile for DT20 in Figure 24(b) now shows a very strong peak at around 125 km.

Strong ionospheric interference at the higher Doppler frequencies has undesirable effects on the detection of aircraft targets such as the CP-121 Tracker. The signal of the Tracker appears in the same Doppler intervals as the interference. Initially, the large samples due to the interference were thought to be the signals of the Tracker aircraft. However, after extensive application of the tracking algorithm, no conclusive tracks could be established.

(d) Slow Roll-off of Sea-Clutter Continuum at Close-in Ranges

As shown in Figure 6(b), the slow roll-off of the Doppler spectrum from the Bragg lines and the spectral replicas at ±5 Hz could raise the noise power-density estimates P_n at close-in ranges. Hence, weak target signals may become undetected because of the slow roll-off at close-in ranges.

The slow roll-off may also cause false alarms at close-in ranges. The statistics of sea clutter is not considered in the detection algorithm. Therefore, when the sea-clutter continuum rolls off slowly into the Doppler regions beyond ±1 Hz, degradation of false-alarm rate is expected.

False tracks will be formed at the close-in ranges as a result of the increased false alarm rate. However, these tracks normally do not follow the fundamental physics: the range increments along these tracks normally do not agree with the distance estimated from the Doppler frequency. Therefore, most of the false tracks can be eliminated in the tracking process with the help of a human operator.

(e) Interference of Unknown Origin

Figure 23(c) shows some of the target-like signals that might be caused either by external interference or by other system operations. These signals very likely result in false alarms.

In addition to these signals, the data may also be disturbed locally in the two-dimensional space of range and time. In Figure 23(d), for example, there are four spectral peaks that exceed the threshold values set by the detection algorithm. These four spectral peaks, at about -3.9, -1.7, -1.05 and 1.3 Hz respectively, indicate the possible presence of four targets in the range cell at the time. However, the tracking algorithm reveals that only the spectral peak at -1.7 Hz is a possible target. The other three are just false alarms that exist in isolation in the two-dimensional space of range and time.

6. Conclusions and Recommendations

From the analysis of the experimental HFSWR data, we have demonstrated some of the radar's capabilities for detecting aircraft targets. At close-in ranges, the radar can easily detect and track the Aurora aircraft, which has a tail-on RCS of about 8.6 dBm^2. At far ranges, up to 280 km, the radar can detect and track some trans-Atlantic commercial aircraft. It was also shown that the radar can track some of the commercial aircraft in the two-dimensional space of range and azimuth if the aircraft are assumed to have constant headings and elevations.

The Tracker aircraft, however, cannot be detected from the experimental data because of its small size and slow speed. The smaller and slower aircraft has a Doppler shift close to the dominating sea-clutter continuum. Consequently, it may have been overshadowed by the sea-clutter continuum in the Doppler spectrum. A HFSWR with a higher operating frequency can probably detect the aircraft since a shorter wavelength implies a larger Doppler separation between the target and the dominant sea-clutter continuum (f vs. $\sqrt{f}$ relationships).

Various interference exist in the HFSWR data. The noise spikes are the most detrimental to target detection, in particular, in the case of turning targets. Better instrumentation is required to reduce the occurrence of the noise spikes in future HFSWR experiments. The 60 Hz harmonic interference does not have a significant effect on the aircraft detection mainly because we have focused on the Doppler frequency intervals away from the spectral peaks. However, it does contaminate the noise statistics in the data and possibly raises the noise floor in the Doppler spectrum. It is necessary to suppress the interference in future HFSWR experiments to obtain the noise statistics. The ionospheric reflection will probably be inherent in the current HFSWR system. However, as pointed out in [3], it is necessary to acquire more data before 10:00 and after 18:00 to investigate the severity of the ionospheric interference, in particular, regarding to its extensiveness in both range and Doppler. This investigation could aid the design of new receive systems that are less susceptible to the interference. The target-like signals due to either external interference or system operations will cause false alarms although the spatially isolated disturbance can be mostly eliminated by the tracking algorithm.

References

1. A.M. Ponsford and S.K. Srivastava, "Ground Wave Radar Development at NORDCO Limited - Phase 1", NORDCO Contract Report, 1990.
2. H.M. Finn and R.S. Johnson, "Adaptive Detection Mode with Threshold Control as a Function of Spatially Sampled Clutter-level Estimates", RCA Review, No. 29, 1968.
3. H.C. Chan, "Long Range Ship Detection Using High Frequency Surface Wave Radar", DREO Report No. 1184, Defence Research Establishment Ottawa, Sept. 1993.
4. D.E. Barrick, J.M. Headrick, R.W. Bogle and D.D. Crombie, "Sea Backscatter at HF: Interpretation and Utilization of the Echo", Proceedings of IEEE, Vol. 62, No. 6, June 1974, pp.673-680.
5. S. K. Srivastava and J. Walsh, "An Analysis of the Second-Order Doppler Return from the Ocean Surface", IEEE J. Ocean Eng., Vol. OE-10, No. 4 pp. 443-445, 1985.
6. H.C. Chan, "Development of Software and Preliminary Analysis of High Frequency Surface Wave Radar Data", DREO Report No. 1153, Defence Research Establishment Ottawa, Dec. 1992.
7. F.J. Harris, "On the Use of Windows for Harmonic Analysis with the Discrete Fourier Transform", Proceedings of the IEEE, Vol. 66, No. 1, pp. 51-83, Jan. 1966.
8. S. K. Srivastava, "Scattering of High-Frequency Electromagnetic Waves from an Ocean Wave: an Alternate Approach Incorporating a Dipole Source", Ph. D. Thesis, Memorial University of Newfoundland, St. John's, Canada, 1984.
9. D. Friend, "The HF Radar Look-up Table Program User's Manual", Version 2-000, DREO Contract Report from Atlantis Scientific, Ottawa, Ontario, Dec. 1993.
10. J.M. Headrick, "HF Over-The-Horizon Radar", in "Radar Handbook", Second Edition, Edited by M. Skolnik, McGraw-Hill Book Company, 1990.
11. A.V. Oppenheim and R.W. Schafer, "Digital Signal Processing", p.28, Prentice-Hall, Inc., New Jersey, 1975.
12. H. Leong, "Suppression of Power Line Harmonic Interference in HF Surface Wave Radar", DREO Report No. 1137, Defence Research Establishment Ottawa, Dec. 1992.
13. S. K. Srivastava and A. M. Ponsford, "Verification of Additional Sea Clutter From a Groundwave Radar", Second Annual TRIO/CRL Radar Symposium, McMaster University, 1989.

14. D. E. Barrick, "Remote Sensing of Sea State by Radar", Chapter 12, in "Remote Sensing of Troposphere", Edited by V. E. Derr, GPO, Washington, DC, 1972.
15. E.D.R. Shearman, "Radio Science and Oceanography", Radio Science, Vol. 18, No. 3, pp. 299-320, 1983.
16. M. Skolnik, "Introduction to Radar Systems", Second Edition, p.449, McGraw-Hill Book Company, 1980.
17. C.C. Teaque, G.L. Tyler and R.H. Stewart, "The Radar Cross Section of the Sea at 1.95 MHz: Comparison of in-situ and Radar Determinations", Radio Science, Vol. 10, No. 10, pp. 847-852, 1974.

Acknowledgement

The author would like to thank Dr. H. C. Chan for his ongoing advice, and Drs. T. Coyne and A. M. Ponsford for their advice on the estimation of the RCS of the CP-140 Aurora.

Appendix: Data Log

Date: August 21, 1989 Note: Newfoundland Time (NDT) is 2:30 behind Greenwich Time (GWT).

File Name	Finish Time (NDT)	Dwell Time (s)	Tape No.	File No.	Comments
DT01	1018	1200	3	1	
DT02	1039	1200	3	2	
DT03	1100	1200	3	3	Tracker over site: 10:40 - in; 10:45 - out
DT04	1125	1200	3	4	Tracker departs
DT05	1146	1200	3	5	Only first 10920 samples are valid; Bluethroat (BTHT) finishes Run#1 and Starts Run#2
DT06	1219	1200	3	6	Aurora over site @start
DT07	1245	1200	3	7	No Bragg; Aurora cross beam @15nm, 200s into data, cuts beam @30nm; Both aircraft 800s into file.
DT08	1303	1200	3	8	TCU Problems; Aurora starts Run#1 at 120s into data, banks at 550s; TCU malfunctions with 468s remaining.
DT15	1444	1200	4	1	Aurora starts Run#3 from 6 to 30 nm with bank 1023s remaining; Tracker departs 750s remaining; BTHT semi-circle turns 555s remaining.
DT16	1506	1200	4	2	
DT17	1526	1200	4	3	BTHT truns to radar 15° off boresight, 272° 1nm with 384s remaining; turns to original course 120s remaining.
DT18	1548	1200	4	4	
DT19	1619	1200	4	5	BTHT steams away for 5 min. at begining; goes to arc with 830s remaining; Tx off 600s remaining.
DT20	1753	1200	5	1	Before contact with BTHT.
DT21	1831	1200	5	3	Contact BTHT restored, 7nm south 500s remaining; steam toward radar for 5 min. (318° True, 24.2nm); 200-180s remaining: returns to original track.

Date: August 22, 1989

File Name	Finish Time (NDT)	Dwell Time (s)	Tape No.	File No.	Comments
DT24	0743	1200	6	2	BTHT commences Run#1
DT25	0805	1200	6	3	
DT26	0826	1200	6	4	
DT27	0847	1200	6	5	
DT28	0922	1200	6	6	BTHT@30nm; Tracker commences Run.
DT29	0943	1200	6	7	800s remaining: Tracker Run T5 commences.
DT30	1003	1200	6	8	
DT31	1024	1200	6	9	184s remaining: Run T5 completed.
DT32	1045	1200	6	10	Run T6 begins with 1150 remaining; BTHT @ 5 knots 1066s remaining, on horizon 550s remaining.
DT33	1125	1200	6	11	720s remaining: BTHT completed Run#1 (1045s ship time); 680s remaining: T6 completed; 560s remaining: BTHT commences RUN#3; 338s remaining: Tracker on site; 230s remaining: T7 starts.
DT34	1146	1200	6	12	
DT37	1248	1200	7	2	BTHT broadside at start; 755s remaining: stern on, stopped till 450s remaining.
DT39	1432	1200	7	4	BTHT broadside till 900s remaining; stern on 865-600s remaining; Tracker starts zigzag run with 1032s remaining.

Date: August 23, 1989

File Name	Finish Time (NDT)	Dwell Time (s)	Tape No.	File No.	Comments
DT46	0824	1200	10	1	Antenna 8 disconnected.
DT47	0856	1200	10	2	Antenna 8 disconnected.
DT48	0954	1200	10	3	Antenna 8 disconnected.
DT49	1025	1200	10	4	Antenna 8 disconnected; BTHT @60nm; 2 ships confirmed at 10:20.
DT50	1115	1200	10	5	Antenna 8 reconnected at start.
DT51	1136	1200	10	6	
DT52	1158	1200	10	7	
DT53	1230	1200	10	9	BTHT @48nm, speed 10 knots (12:10).
DT55	1259	1200	10	12	
DT56	1323	1200	10	13	
DT57	1357	1200	10	14	
DT60	1513	650	10	17	

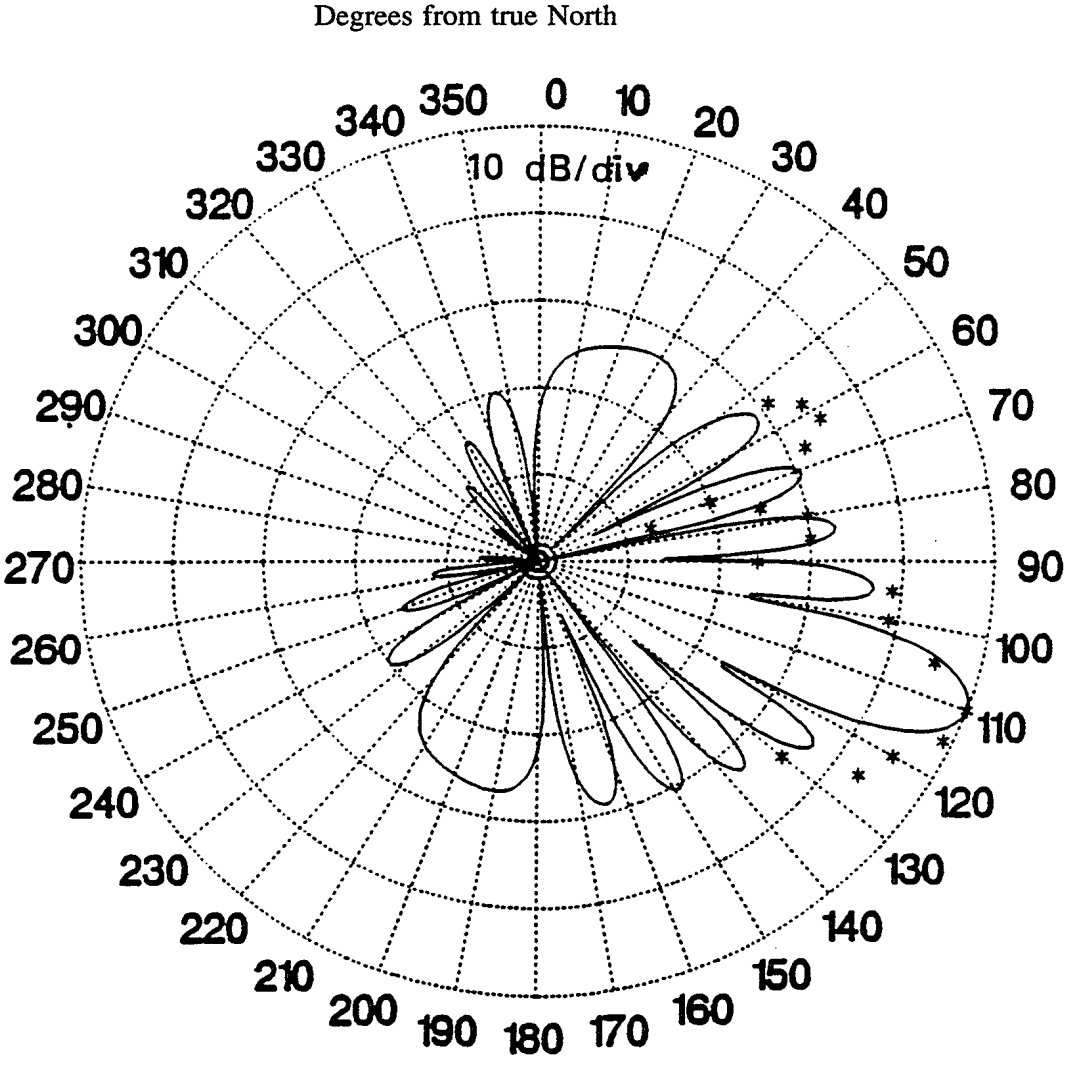

Figure 1 Theoretical and Measured Beam Pattern of Receiver Array (Reproduced from [1])

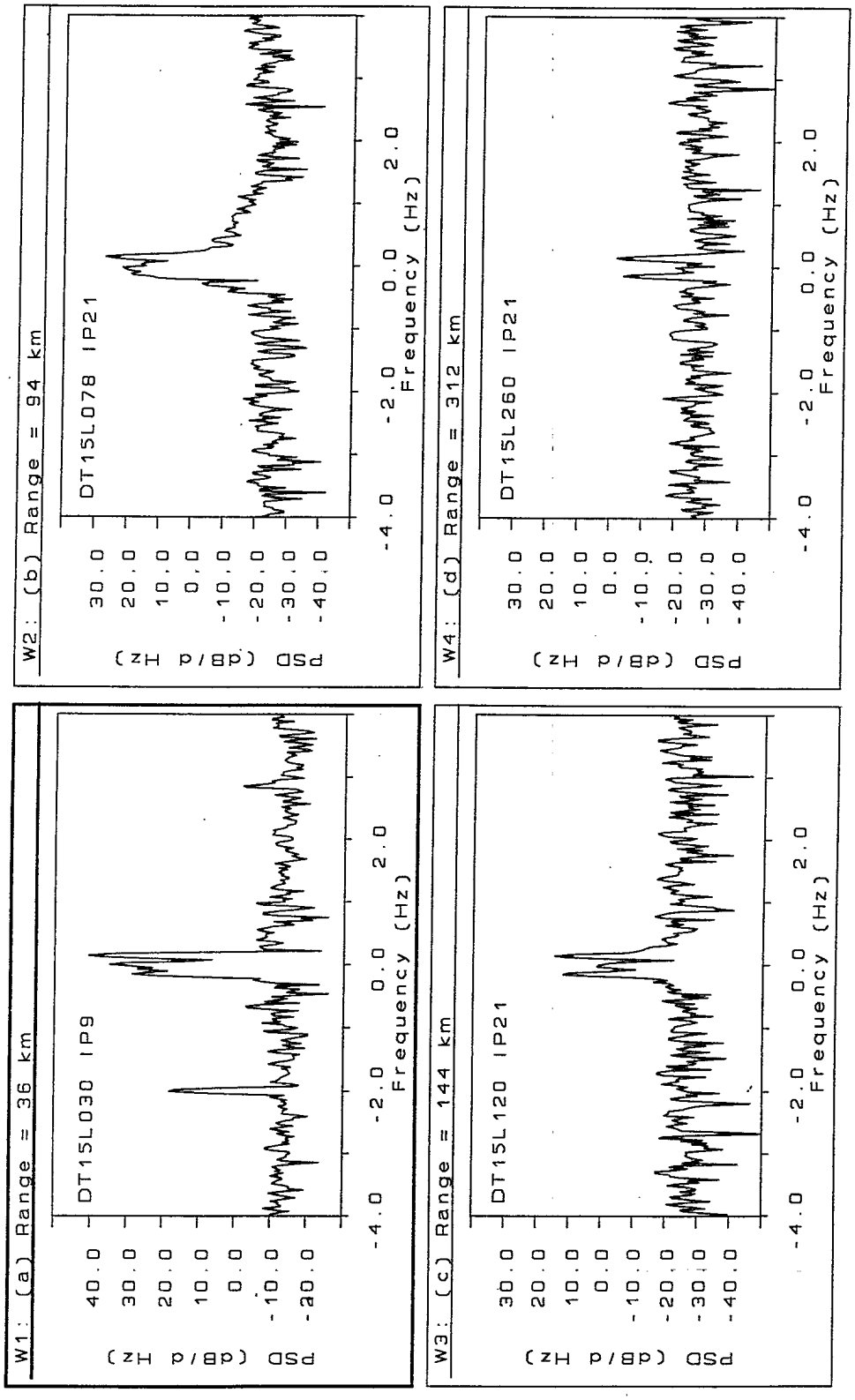

Figure 2 Doppler Spectra of the HFSWR Time Series at Various Ranges

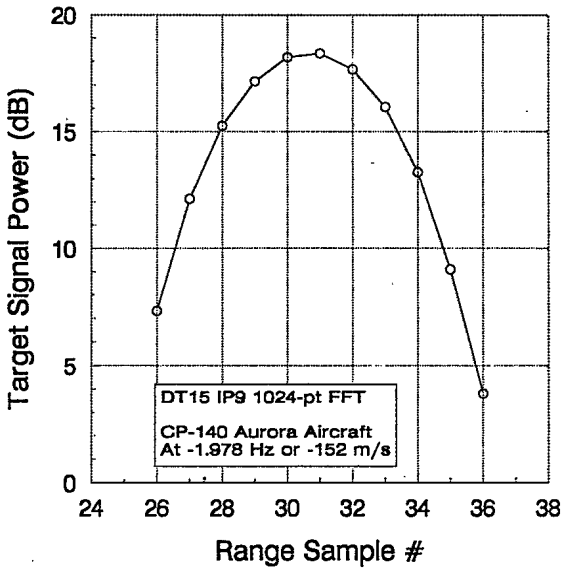

Figure 3 Interpolation of Target Signal Across Range

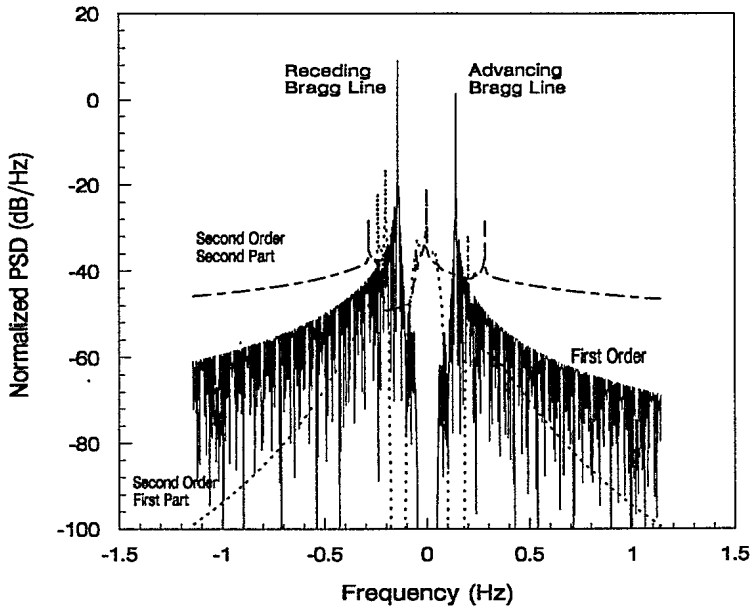

Figure 4 Theoretical Spectra of Sea Clutter from 1.95 MHz HFSWR under a Fully Developed Sea Condition

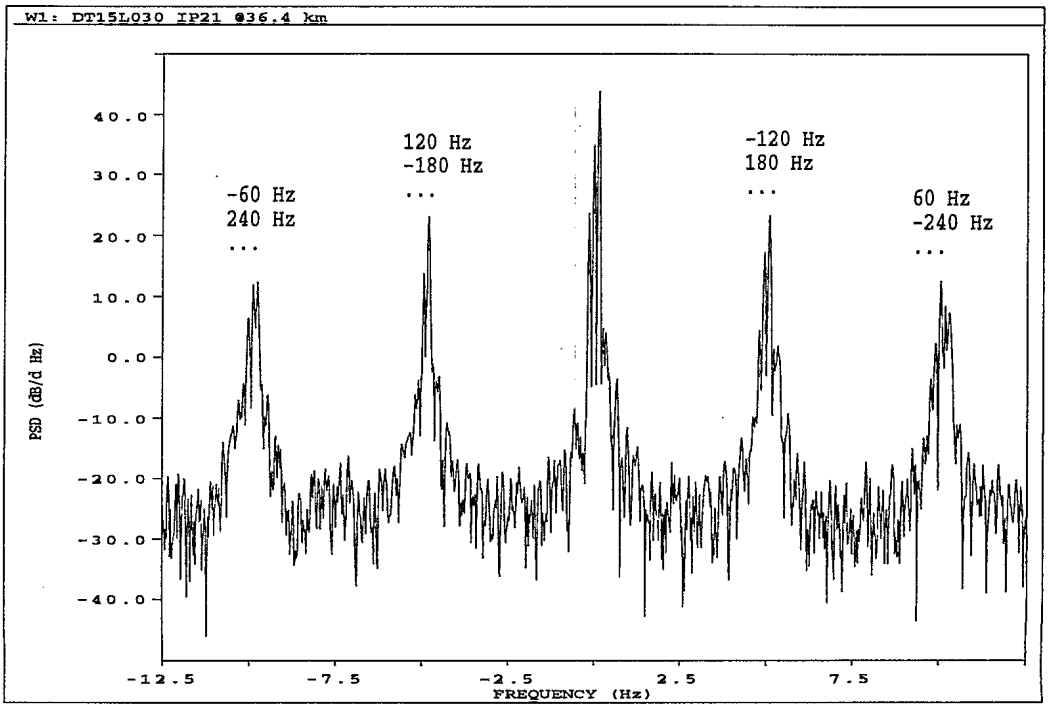

Figure 5 Doppler Spectrum of HFSWR Time Series showing 60 Hz Harmonic Interference

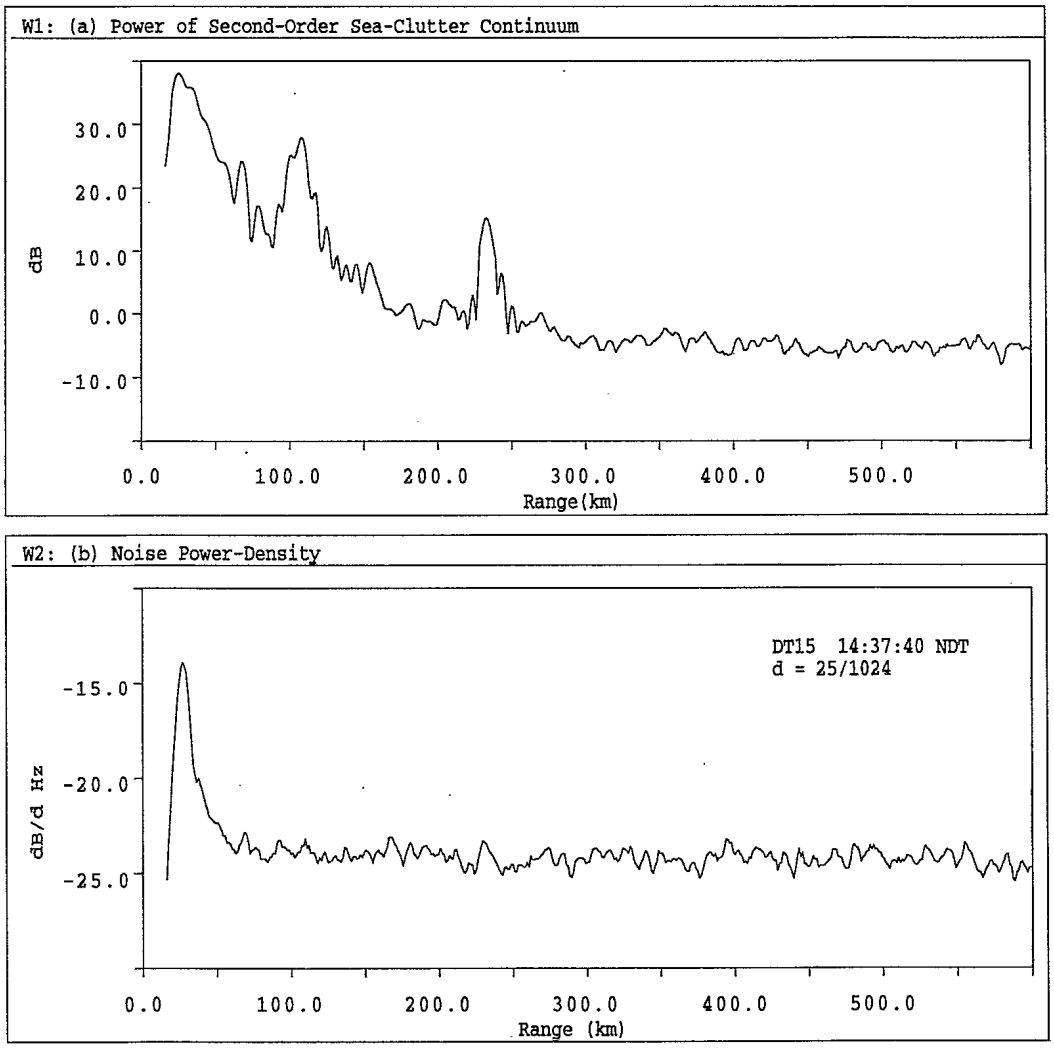

Figure 6 Range Variations of Doppler Components in DT15

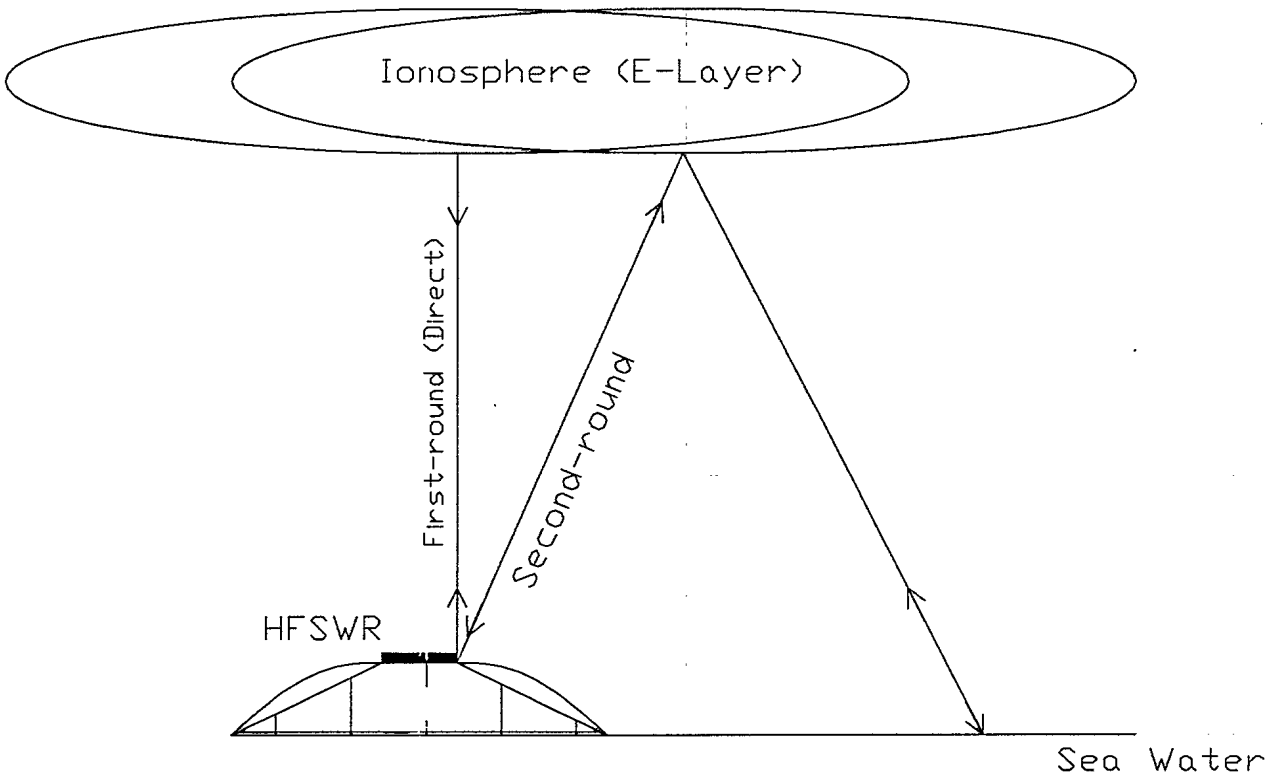

Figure 7 Paths of First-round and Second-round Ionospheric Reflections

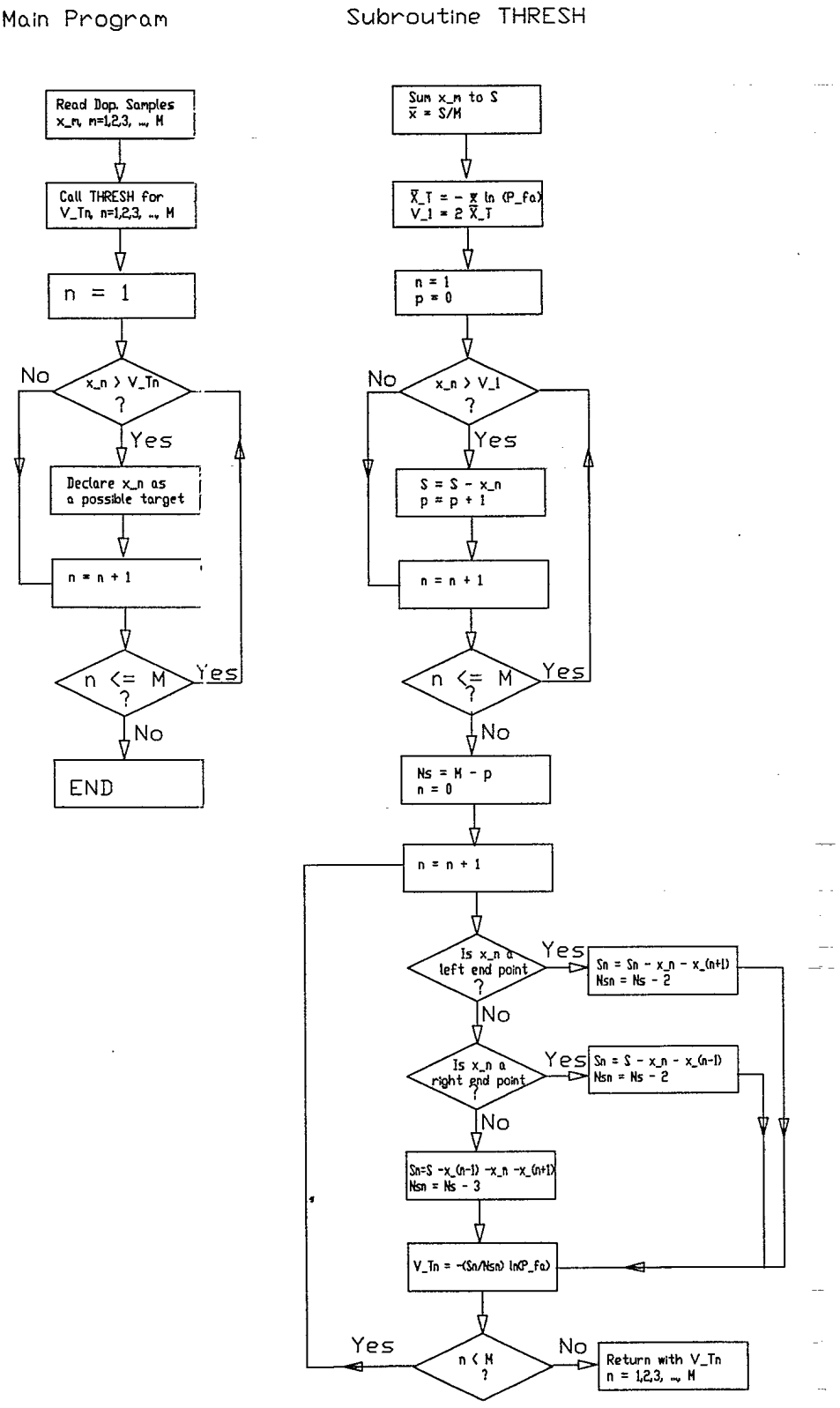

Figure 8 Block Diagram for Detection Algorithm

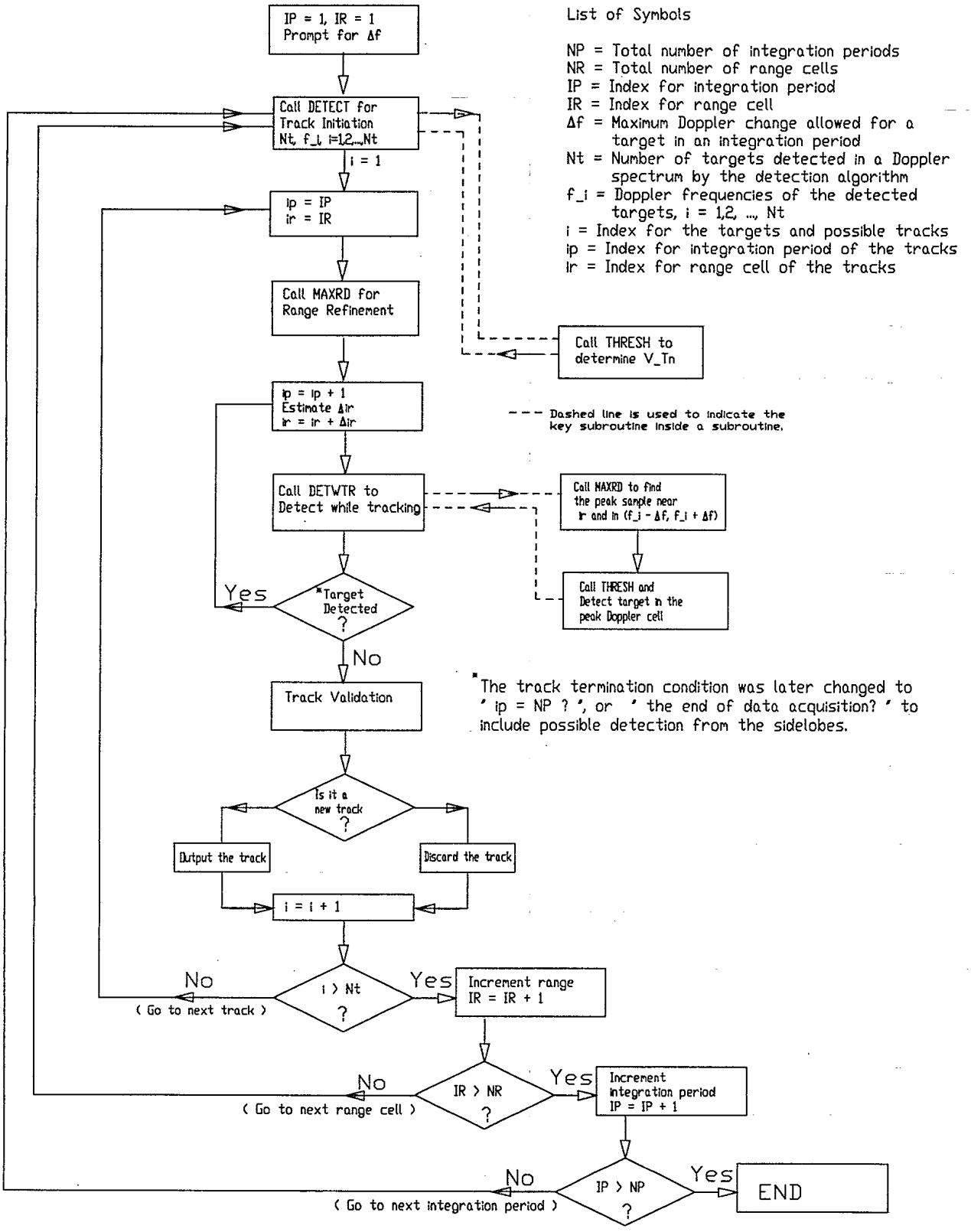

Figure 9 Block Diagram for Tracking Algorithm

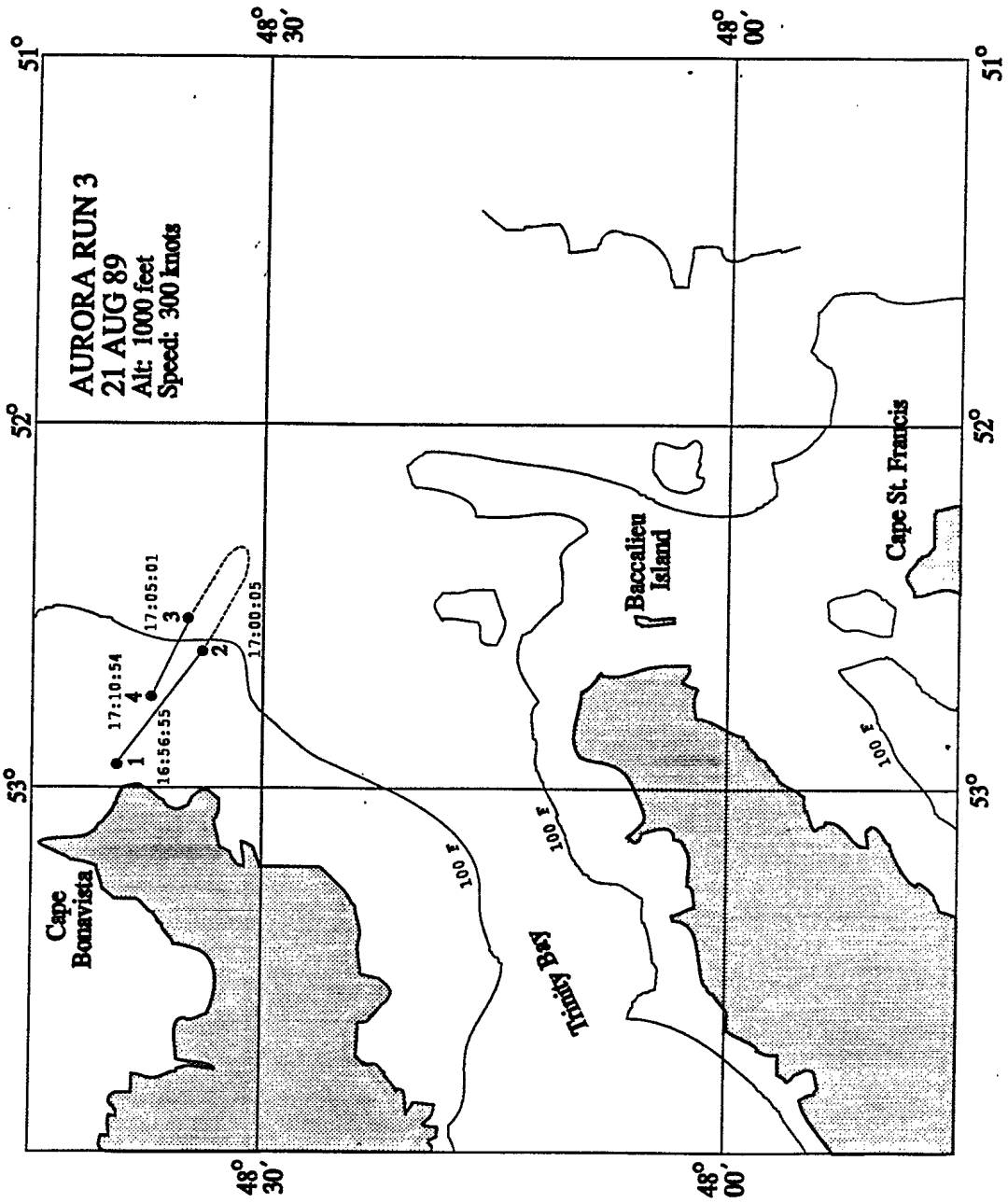

Figure 10 Recorded Track of the CP-140 Aurora Aircraft in Run #3 (Reproduced from [1])

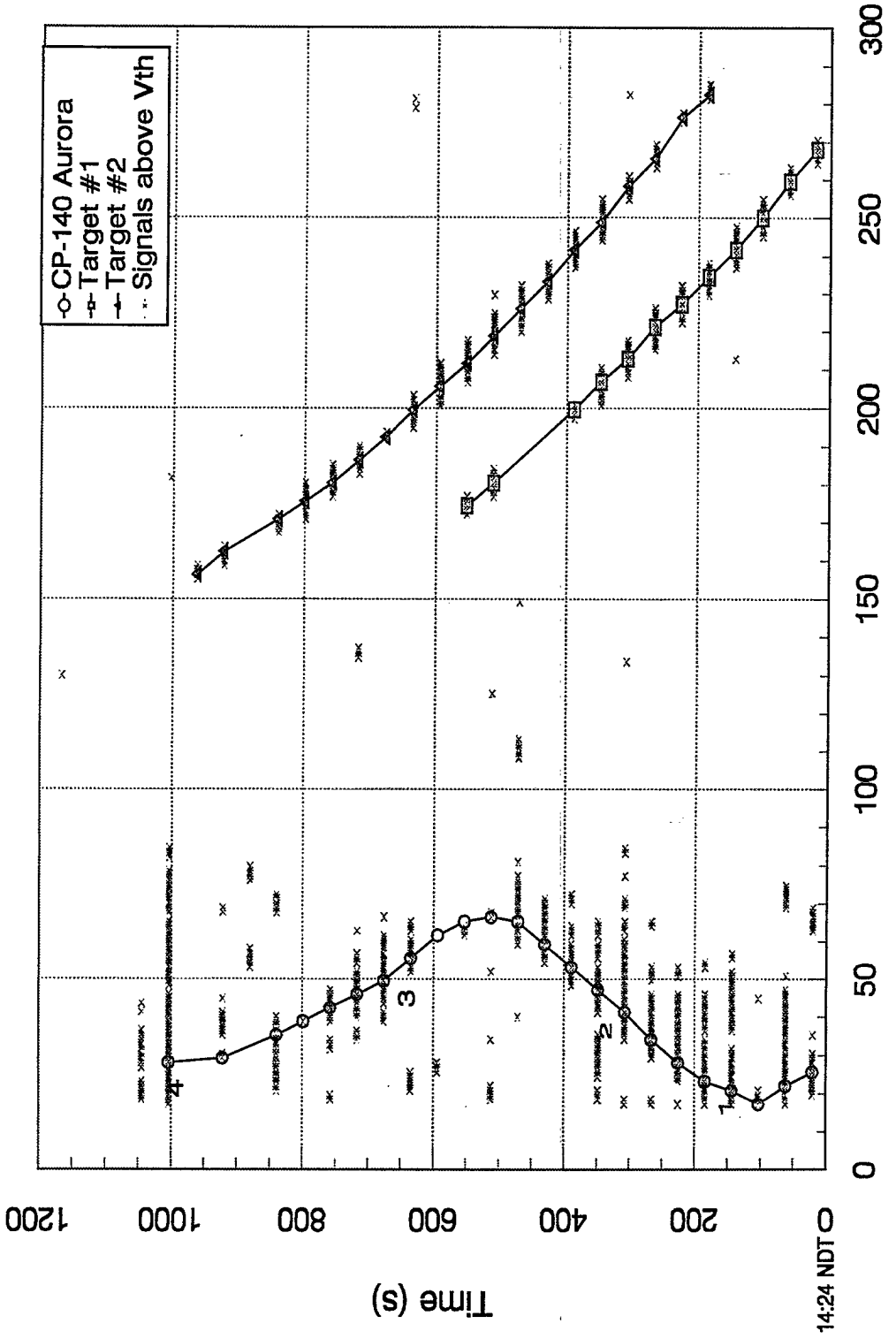

Figure 11 Target Tracks in DT15

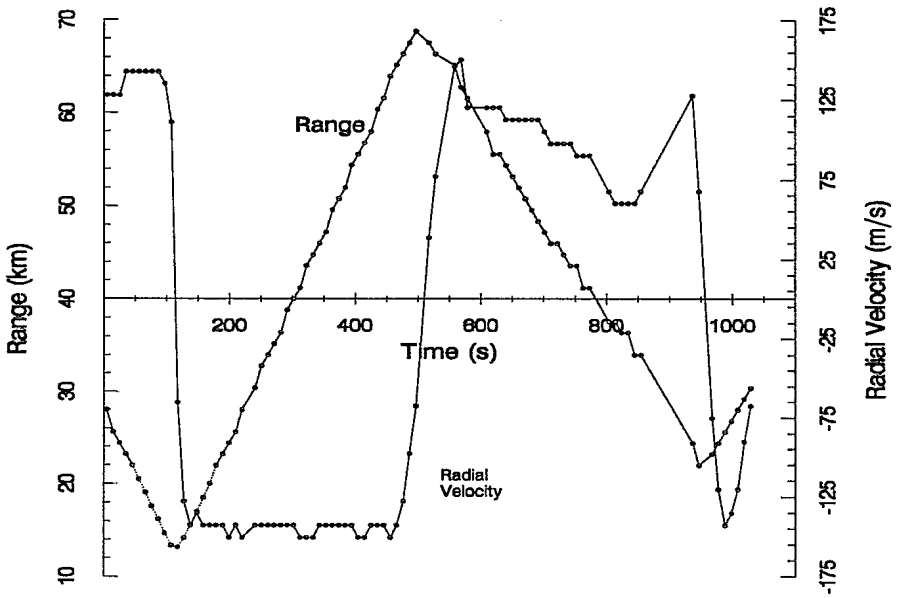

Figure 12 Range and Radial Velocity of the Aurora Aircraft in DT15

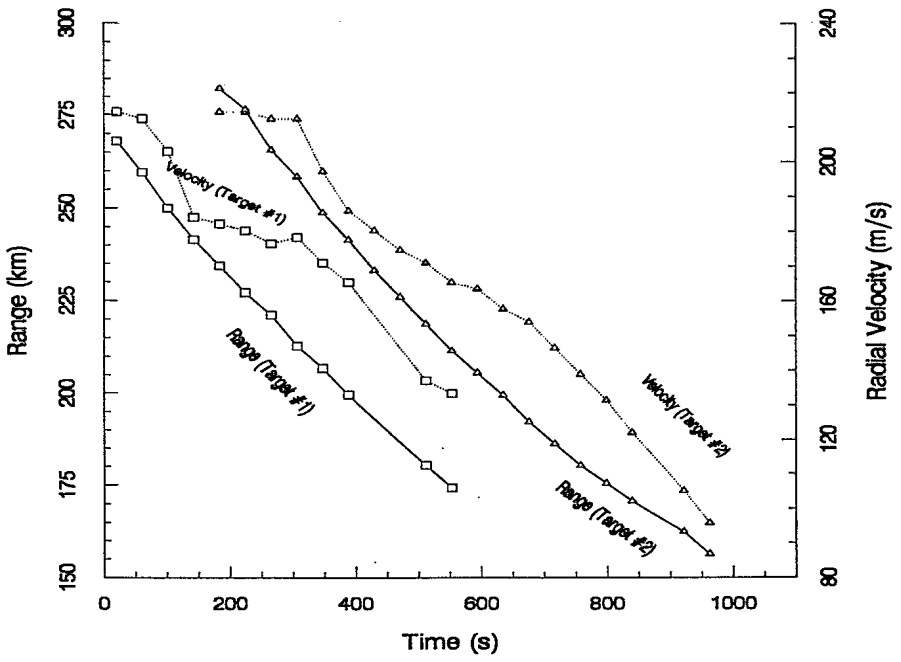

Figure 13 Ranges and Radial Velocities of Target #1 and #2 in DT15

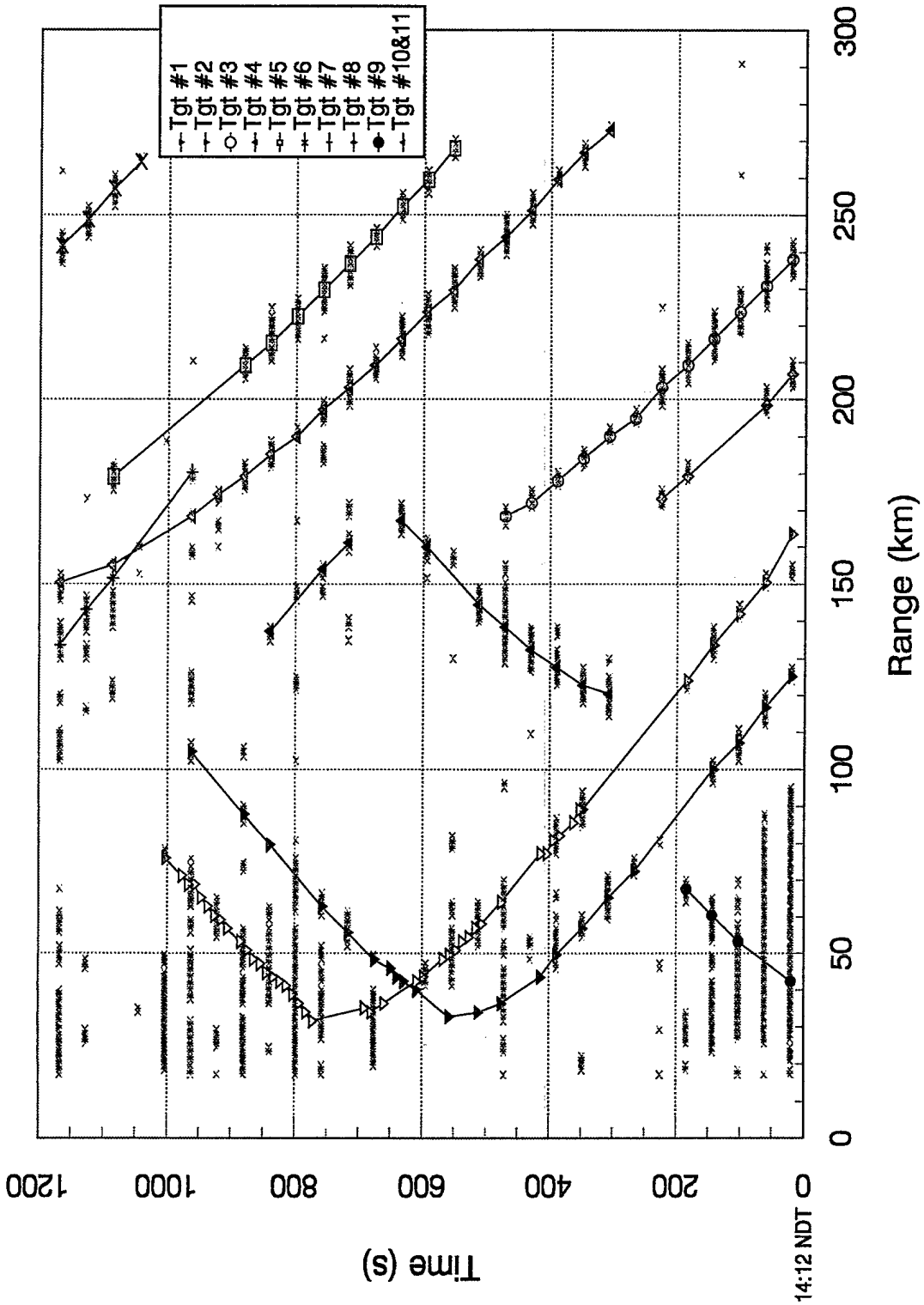

Figure 14 Target Tracks in DT39

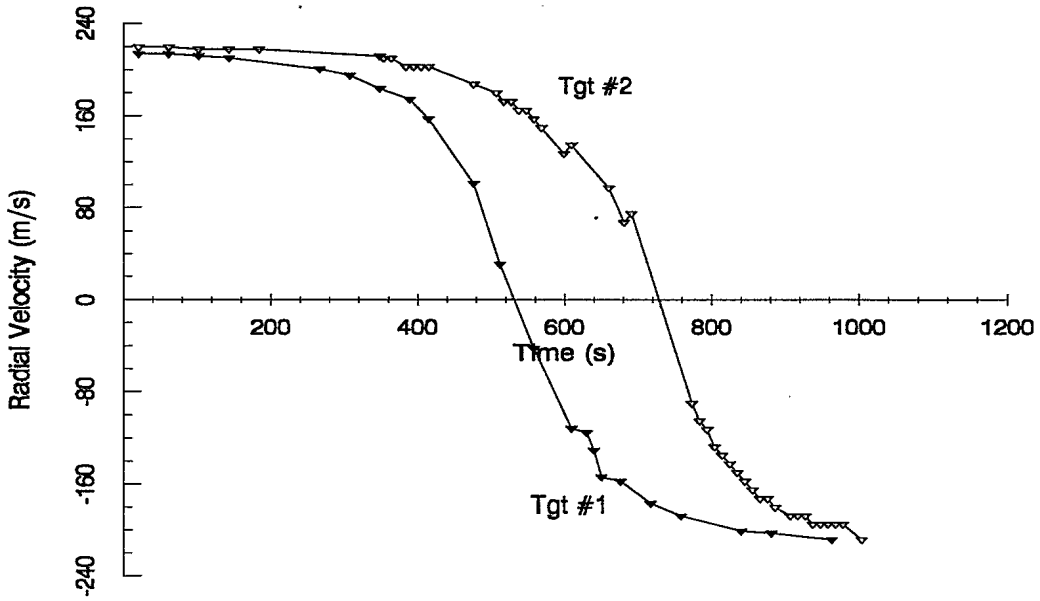

Figure 15 Radial Velocities of Target #1 and #2 in DT39

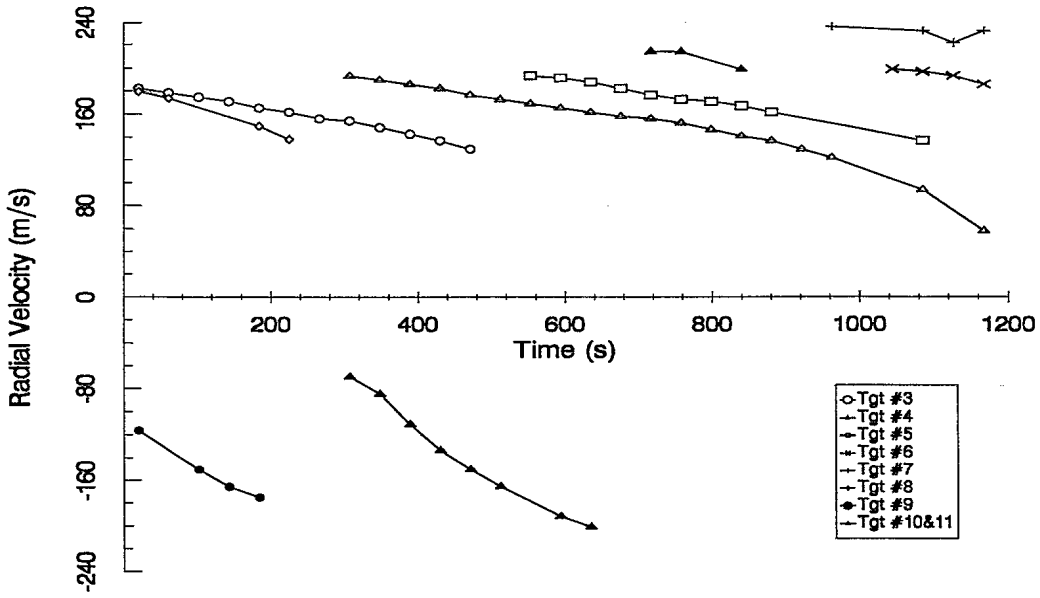

Figure 16 Radial Velocities of the Other Aircraft Targets in DT39

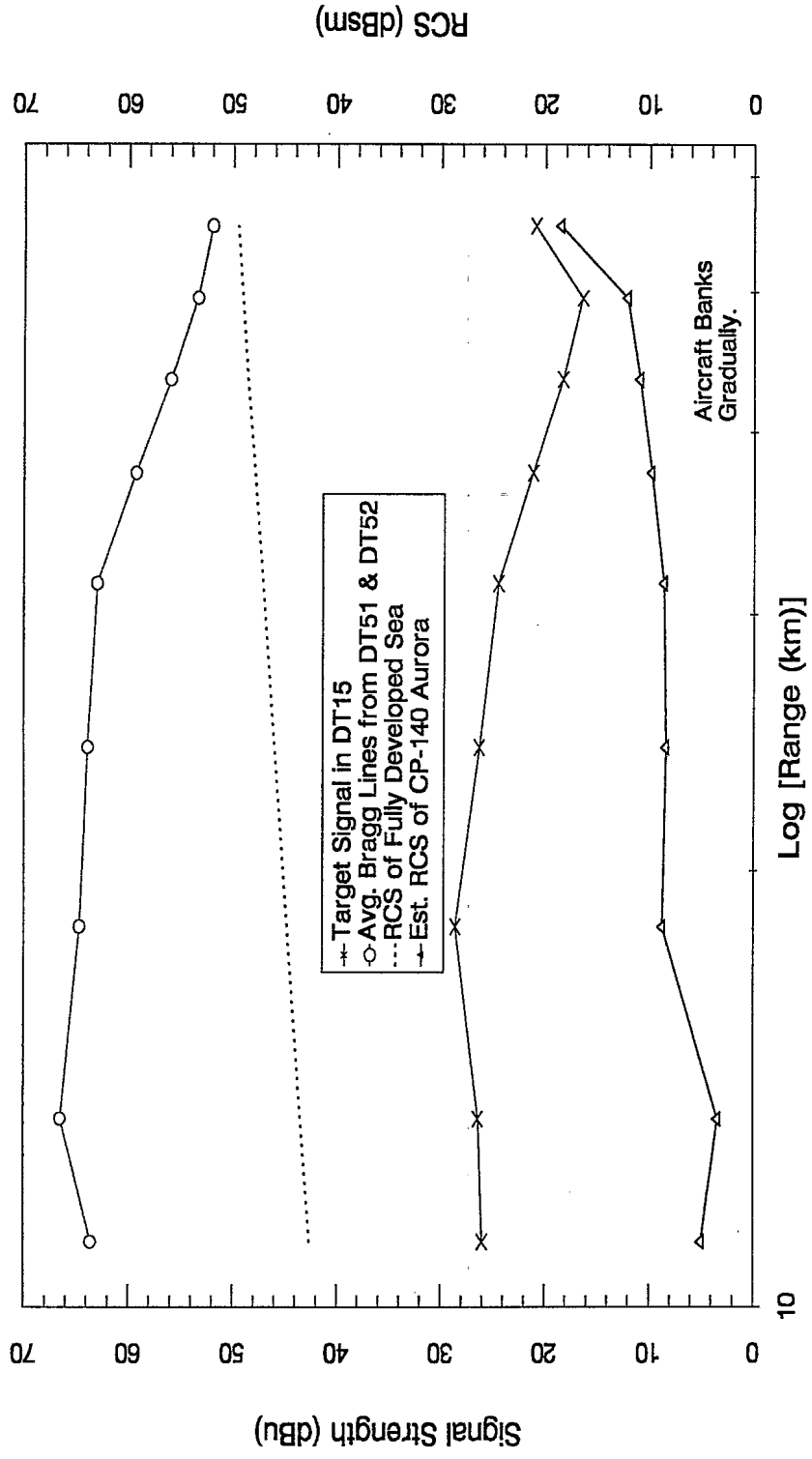

Figure 17 Signal Strengths and RCS Estimates of the CP-140 Aurora and Bragg Lines

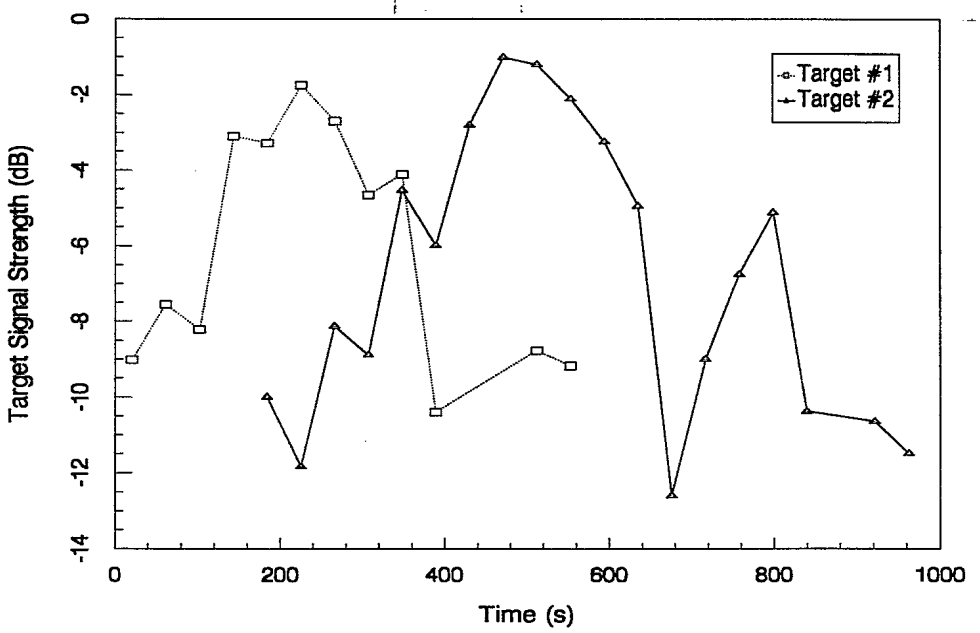

Figure 18 Signal Strengths of Tareget #1 and #2 in DT15

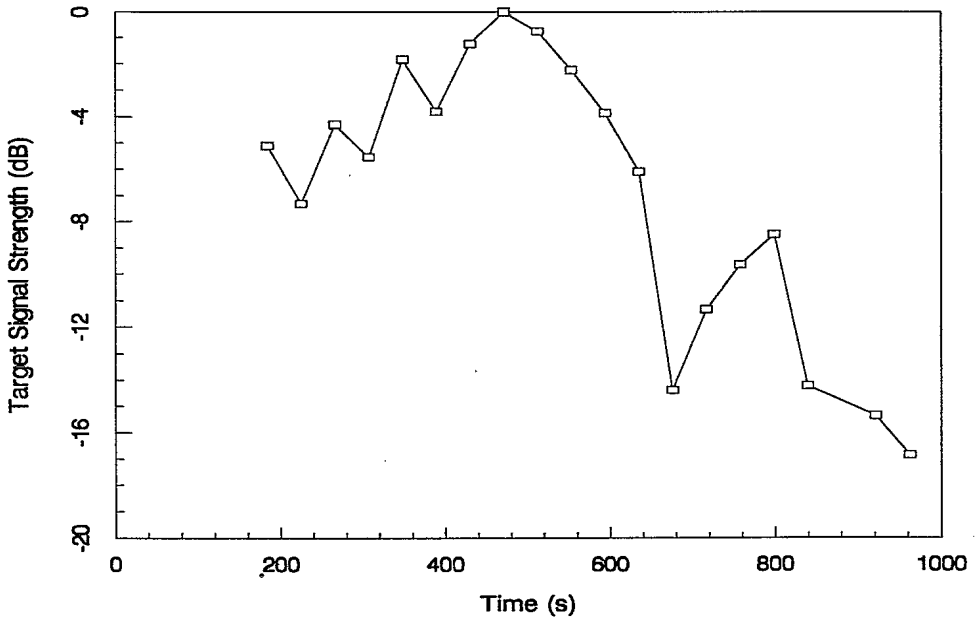

Figure 19 Range-Corrected Signal Strength of Target #2 in DT15 (Normalized to the peak value)

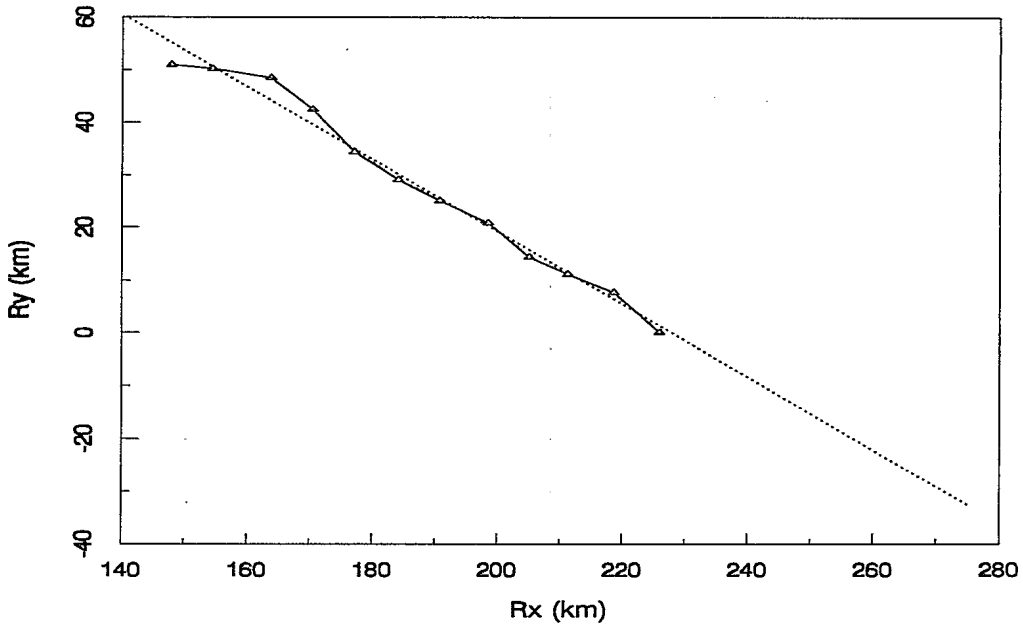

Figure 20 Track of Target #2 in DT15 in the Retangular Coordinates

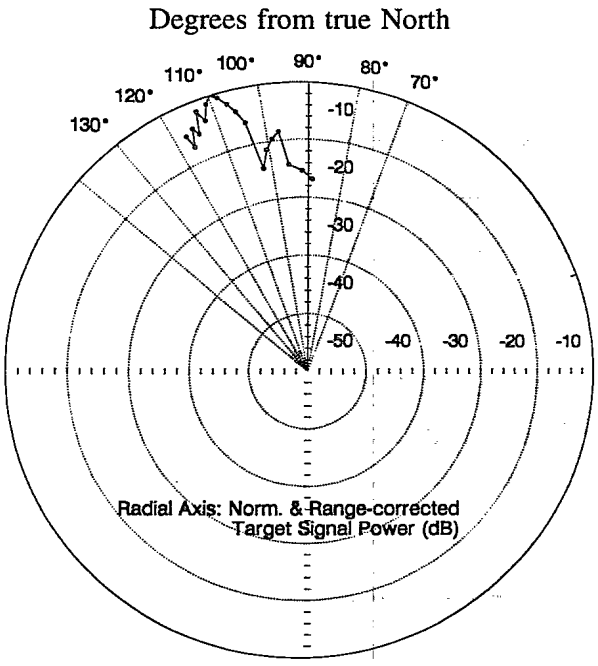

Figure 21 Range-Corrected Signal Strength of Target #2 in the Polar Coordinates

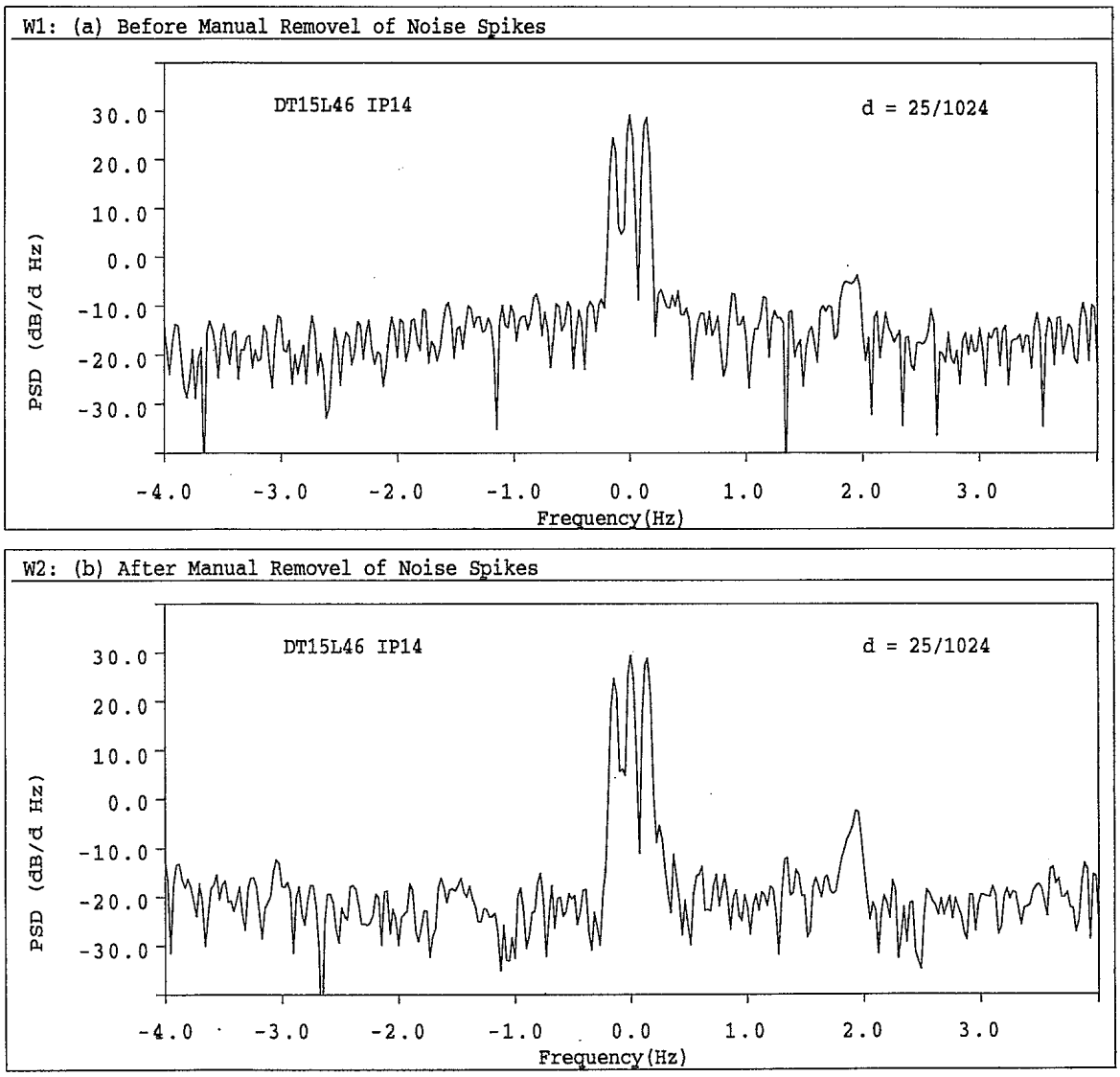

Figure 22 A Doppler Spectrum of DT15 before and after Removal of Noise Spikes

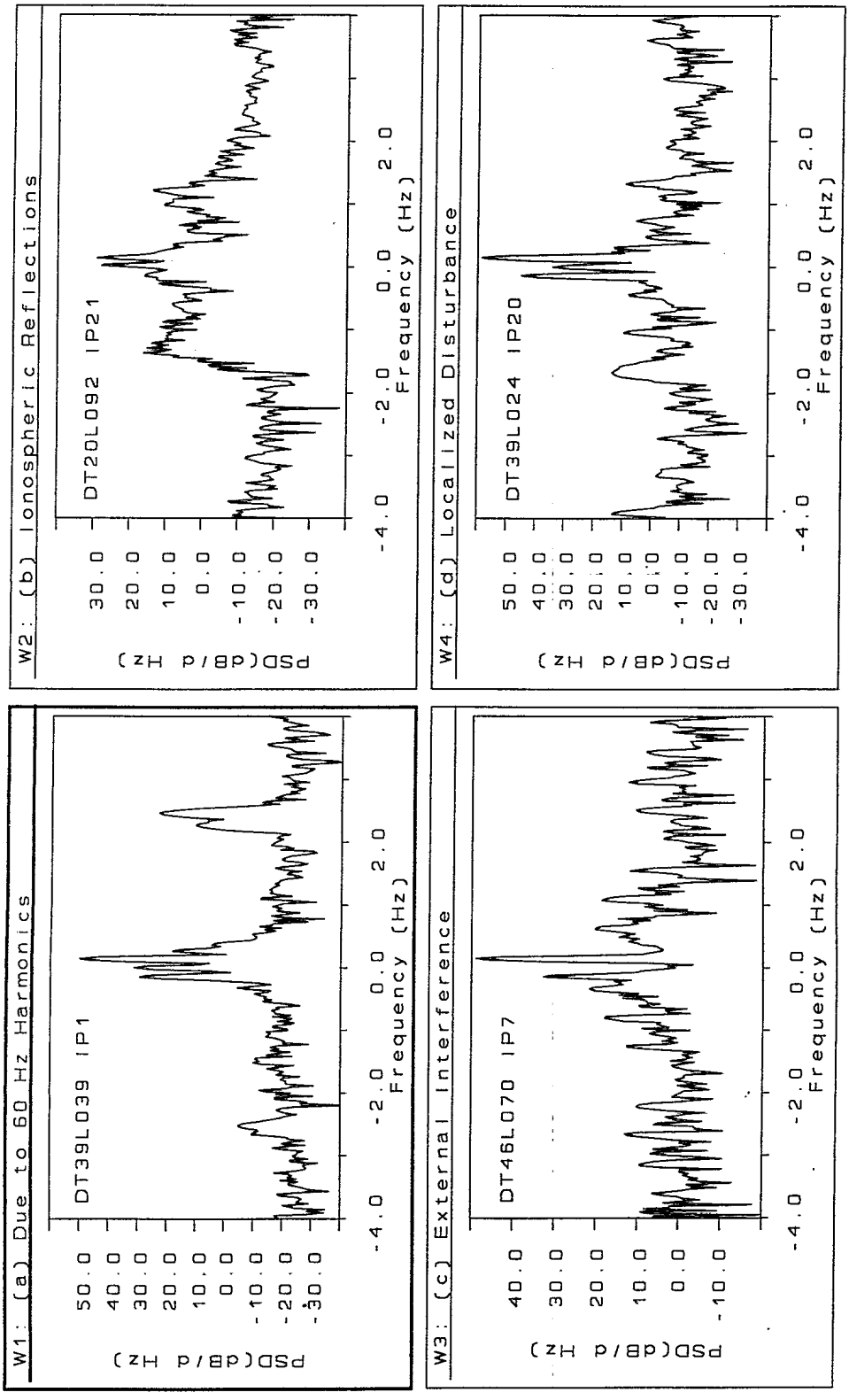

Figure 23 Doppler Spectra of the HFSWR Time Series subject to Various Interference

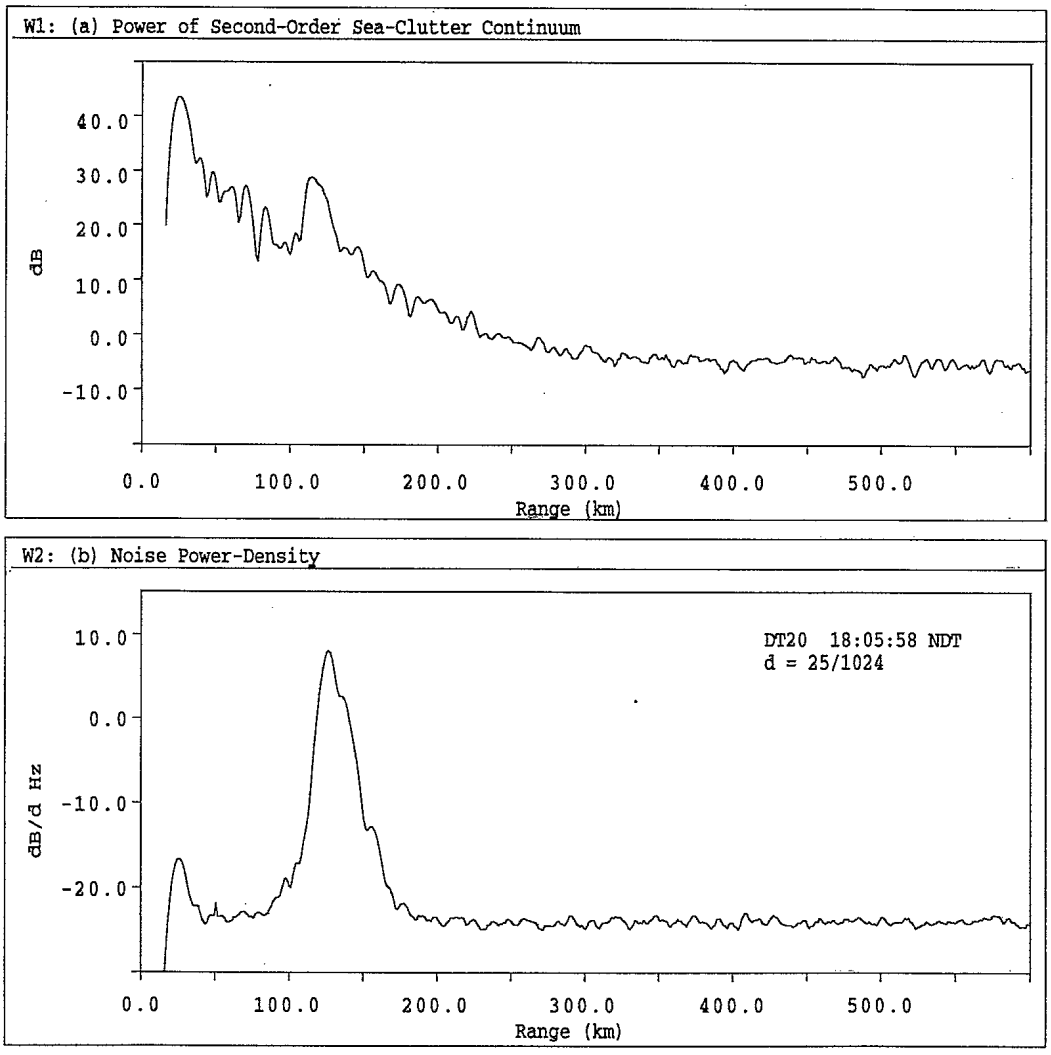

Figure 24 Range Variations of Doppler Components in DT20

DOCUMENT CONTROL DATA

(Security classification of title, body of abstract and indexing annotation must be entered when the overall document is classified)

1. ORIGINATOR (the name and address of the organization preparing the document. Organizations for whom the document was prepared, e.g. Establishment sponsoring a contractor's report, or tasking agency, are entered in section 8.)

DEFENCE RESEARCH ESTABLISHMENT OTTAWA
3701 CARLING AVE. OTTAWA, ONTARIO, K1A 0Z4

2. SECURITY CLASSIFICATION (overall security classification of the document. including special warning terms if applicable)

UNCLASSIFIED

3. TITLE (the complete document title as indicated on the title page. Its classification should be indicated by the appropriate abbreviation (S,C or U) in parentheses after the title.)

LONG RANGE AIRCRAFT DETECTION USING HIGH-FREQUENCY SURFACE-WAVE RADAR (U)

4. AUTHORS (Last name, first name, middle initial)

LEONG, HANK W. H.

5. DATE OF PUBLICATION (month and year of publication of document)

DECEMBER, 1994

6a. NO. OF PAGES (total containing information. Include Annexes, Appendices, etc.)

55

6b. NO. OF REFS (total cited in document)

17

7. DESCRIPTIVE NOTES (the category of the document, e.g. technical report, technical note or memorandum. If appropriate, enter the type of report, e.g. interim, progress, summary, annual or final. Give the inclusive dates when a specific reporting period is covered.)

TECHNICAL REPORT

8. SPONSORING ACTIVITY (the name of the department project office or laboratory sponsoring the research and development. Include the address.)

DEFENCE RESEARCH ESTABLISHMENT OTTAWA
3701 CARLING AVE. OTTAWA, ONTARIO, K1A 0Z4

9a. PROJECT OR GRANT NO. (if appropriate, the applicable research and development project or grant number under which the document was written. Please specify whether project or grant)

041LR

9b. CONTRACT NO. (if appropriate, the applicable number under which the document was written)

10a. ORIGINATOR'S DOCUMENT NUMBER (the official document number by which the document is identified by the originating activity. This number must be unique to this document.)

DREO REPORT No. 1245

10b. OTHER DOCUMENT NOS. (Any other numbers which may be assigned this document either by the originator or by the sponsor)

11. DOCUMENT AVAILABILITY (any limitations on further dissemination of the document, other than those imposed by security classification)

- (X) Unlimited distribution
- ( ) Distribution limited to defence departments and defence contractors; further distribution only as approved
- ( ) Distribution limited to defence departments and Canadian defence contractors; further distribution only as approved
- ( ) Distribution limited to government departments and agencies; further distribution only as approved
- ( ) Distribution limited to defence departments; further distribution only as approved
- ( ) Other (please specify):

12. DOCUMENT ANNOUNCEMENT (any limitation to the bibliographic announcement of this document. This will normally correspond to the Document Availabilty (11). However, where further distribution (beyond the audience specified in 11) is possible, a wider announcement audience may be selected.)

UNLIMITED

13. ABSTRACT (a brief and factual summary of the document. It may also appear elsewhere in the body of the document itself. It is highly desirable that the abstract of classified documents be unclassified. Each paragraph of the abstract shall begin with an indication of the security classification of the information in the paragraph (unless the document itself is unclassified) represented as (S), (C), or (U). It is not necessary to include here abstracts in both offical languages unless the text is bilingual).

Experimental data from a High-Frequency Surface-Wave Radar (HFSWR) operating at 1.95 MHz at Cape Bonavista, Newfoundland are analyzed to assess the capability of the radar to detect aircraft over an ocean surface. The results of the analysis show that the HFSWR could easily detect and track a low-flying CP-140 Aurora aircraft at ranges between 11 and 56 km. The radar's coverage area coincides with a trans-Atlantic international flight route, and the radar was also able to detect and track some commercial aircraft in range as far as 280 km.

14. KEYWORDS, DESCRIPTORS or IDENTIFIERS (technically meaningful terms or short phrases that characterize a document and could be helpful in cataloguing the document. They should be selected so that no security classification is required. Identifiers, such as equipment model designation, trade name, military project code name, geographic location may also be included. If possible keywords should be selected from a published thesaurus. e.g. Thesaurus of Engineering and Scientific Terms (TEST) and that thesaurus-identified. If it is not possible to select indexing terms which are Unclassified, the classification of each should be indicated as with the title.)

HF RADAR, HIGH-FREQUENCY SURFACE-WAVE RADAR, HF GROUNDWAVE RADAR, AIRCRAFT DETECTION